Non peer-reviewed EarthArXiv preprint
Submitted to the journal Geothermal Energy

Repurposing idle wells in the North German Basin as deep borehole heat exchangers

Nora Koltzer*[1] and Johannes Schoenherr[2] and Maximilian Sporleder[3,4] and Jan Niederau[5] and Florian Wellmann[5,6]

[1] Fraunhofer IEG, Fraunhofer Research Institution for Energy Infrastructures and Geothermal Systems IEG, Gulbener Straße 23, 03046 Cottbus, Germany

[2] ExxonMobil Production Deutschland GmbH, Vahrenwalder Straße 238, 30179 Hannover, Germany

[3] Fraunhofer IEG, Fraunhofer Research Institution for Energy Infrastructures and Geothermal Systems IEG, Breslauer Straße 48, 76139 Karlsruhe, Germany

[4] Brandenburg University of Technology Cottbus-Senftenberg BTU, Department of Electrical and Thermal Energy Systems, Cottbus, Germany

[5] Fraunhofer IEG, Fraunhofer Research Institution for Energy Infrastructures and Geothermal Systems IEG, Kockerellstr. 17, 52062 Aachen, Germany

[6] RWTH Aachen University, Institute for Computational Geoscience, Geothermics and Reservoir Geophysics, Mathieustraße 30, 52074 Aachen, Germany

*nora.koltzer@ieg.fraunhofer.de
johannes.schoenherr@exxonmobil.com
maximilian.sporleder@ieg.fraunhofer.de
jan.niederau@ieg.fraunhofer.de
florian.wellmann@ieg.fraunhofer.de, florian.wellmann@cgre.rwth-aachen.de

Abstract. This study investigates the feasibility to repurpose wells from gas production for geothermal closed loop application in the North German Basin (NGB). The objective is to extend the value-added chain of idle wells by re-completion as coaxial deep borehole heat exchangers as an efficient way to produce green energy without drilling new wells by saving the carbon emission and costs of building a new geothermal well.

With numerical models of two typical geological settings of the North German Basin (NGB) and two different completion schemes, it is possible to simulate the thermal performance over a lifetime of 30 years. The calculated heat extraction rates range from 200 kW to 400 kW, with maximum values of up to 600 kW. The heat extraction is higher compared to installed deep borehole heat exchangers. Sensitivity analyses demonstrate that re-completion depth and injection temperature are the most sensitive parameters of thermal output determination.
The heat demand around the boreholes is mapped, and heat generation costs are calculated with heating network simulations. The initial production costs for heat are comparable to other renewable energy resources like biomass and competitive against gas prices in 2023.
This study highlights available geothermal resources' environmental and economic potential in already installed wells. The application has almost no geological and no drilling risks and may be installed at any idle well location.

Keywords: Deep Borehole Heat exchanger, legacy wells, heat generation costs, Feflow, heat demand mapping, coaxial, vacuum insulated tubing, North German Basin, geothermal energy, heat source.

1 Introduction

Energy consumption increases with the increasing number of industrialized countries and population growth (Santos et al. 2022). To guarantee reliable power and heat supply, we will need all possible renewable and climate-neutral energy resources we can think of in the future. Geothermal energy is a critical component of renewable and green energy supply. The heat exists naturally and is stored in the subsurface everywhere in the earth's crust (Sharmin et al. 2023). The deep geothermal resources can be exploited in open systems like hydrothermal doublets, with Enhanced Geothermal Systems (EGS), or through closed-loop systems as borehole heat exchangers (BHE). Open geothermal operations interfere directly with the reservoir fluid and the pore pressure causing higher risks of seismicity, scaling, and corrosion (Gascuel et al. 2022) as well as the classical exploration risks known from hydrocarbon exploration. With deep borehole heat exchangers (deeper than 400 m, DBHE), it is only possible to exploit a fraction of the thermal energy of the earth's crust, but with low-risk and very low maintenance and operational costs. The remaining disproportionate investment costs can be minimized if already existing wells are repurposed as DBHE. This article will discuss how this could become an economically and technically viable concept.

1.1 Deep Borehole Heat Exchangers

The concept of DBHE is not new, but only a few systems are operated worldwide. An overview of worldwide studies of DBHE is given in review papers by e.g.Rashid et al. (2023) and Alimonti et al. (2018; Rashid et al.). The typical completion system in depths higher than 2 km is a coaxial pipe (in contrast to u- shape or double u- shape for shallow BHE). A refrigerant (mostly fluid, sometimes gas) is circulated within the wellbore and transports the heat from depth to the surface (Figure 1**Error! Reference source not found.**). Cool fluid is pumped down in the annulus and is heated on the way down. The heated refrigerant is then pumped upwards through the central tubing. To avoid cooling of the fluid in the central tubing, it is constructed of material with low thermal conductivity (best are vacuum insulated tubings; VIT). Within this study, we make use of the commercial software code FEFLOW (DHI WASY, (Diersch et al. 2011; Diersch et al. 2010)) to numerically solve the heat transport of the DBHE in a 3D porous medium of surrounding rocks. The modelling concept makes it possible to assess parameter variations of the geological uncertainty, re-completion factors, and operational values, as these parameters significantly affect the performance of the DBHE (Rashid et al. 2023).

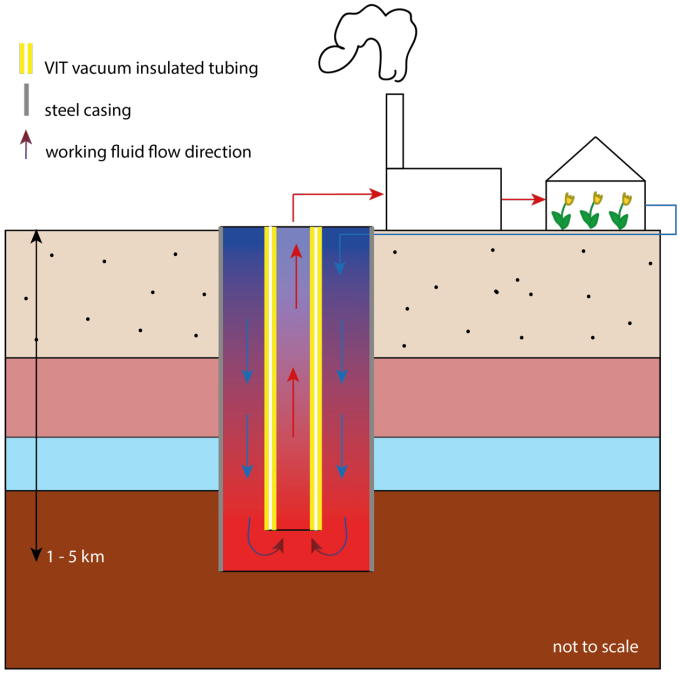

Figure 1: Well design of an illustrative coaxial deep borehole heat exchanger

1.2 Geological setting of two idle well locations

The North German Basin (NGB) is a major hydrocarbon province, with abundant exploration and still active production. Two major play types occur in this system: (1) reservoirs (typically clastic) and traps in normal stratigraphic sequences, and (2) clastic reservoirs and traps related to salt diapir settings. In this work, we will examine one well from each of these settings, in order to obtain representative results that are transferable to similar play types.

The first setting is called as “stratigraphic normal setting” referred to as NS (Figure 2a) and the second is referred to as SD (Figure 2b). Due to extensive salt tectonics in the NGB the thick layer of Zechstein salt is deformed into salt pillows, salt domes and salt diapirs. Due to its high thermal conductivity, vertical aligned salt structures discharge the heat from depths efficiently to shallow formations by conduction and thereby lead to positive thermal anomalies above the salt structures (Fromme et al. 2010). This effect is also called chimney effect and is based on high thermal conductivity contrasts between the salt body (with high values of thermal conductivity) and the surrounding rocks (with lower thermal conductivity). In hydrocarbon systems, salt represents a tight and sealing lithology and therefore idle wells often intersect long salt zones. To investigate the influence of the thermal properties of salt for repurposing idle wells into DBHE, we decided to study one salt diapir (SD).

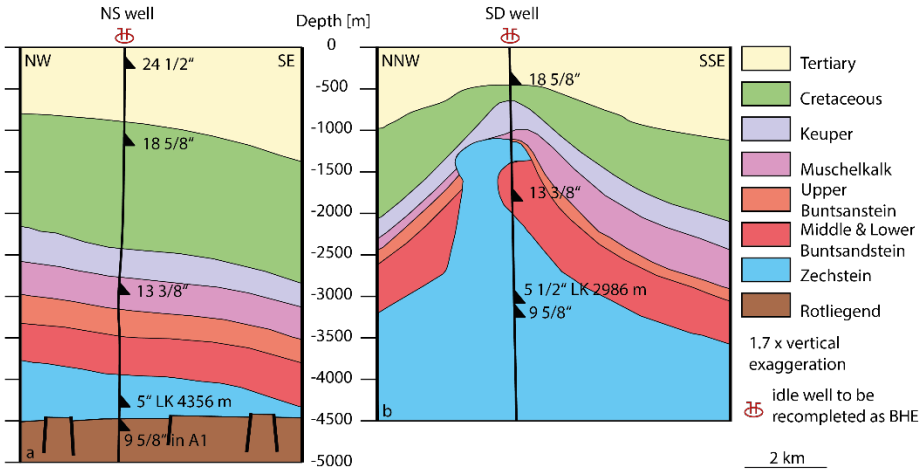

Figure 2: Slice through interpretation of processed 3D seismic cubes from (a) NW to SE through stratigrafic normal setting (NS) and (b) NNW to SSE through a salt diapir (SD). BHE = Borehole heate exchanger, LK = top of liner.

The depth of top and base for each stratigraphic unit for both geological settings are listed in Table 6 and are used to construct the horizontal layers of the 3D numerical models.

2 Methods and data for the subsurface and above surface systems

This study combines detailed investigations of the subsurface system and the above surface infrastructure. The Subsurface part includes the representation of two geological settings as described in the section before and the according different thermal fields with the recompleted idle wells as DBHE. The according subsurface processes and components are investigated based on numerical models built with the software FEFLOW. FEFLOW is a powerful finite element simulation software to calculate fluid flow and heat transport in porous media (FEFLOW 2014). It is widely used within the geothermal community to simulate and predict the power of hydrothermal doublets, the performance of ATES systems and the thermal output of (deep) BHEs (e.g. Wenderoth et al. 2005, Le Lous et al. 2015; Gascuel et al. 2022).
The above surface part is simulated seperately and consists of the heat demand mapping at the two idle well locations at first, followed by the heating grid simulation with the prediction of heat generation costs.

2.1.1 Building the structural models for the subsurface at two locations

For the construction of the models and the simulation of the thermal processes and the BHE application afterwards, the software FEFLOW by DHI Wasy is used. The structural models have the shape of a square box of 1 km by 1 km in lateral extension with the well location in the center. The total depth of the model is for the NS well to 5.5 km below mean sea level and for the SD model 5 km below mean sea level. The uppermost slice reflects the elevation of the topography (Houska 2012) and all other layers are subhorizontal and parallel. The depths of the stratigraphic units were taken from the well tops and are listed in Table 6 (in Supplementary Material S1). The horizontal mesh resolution varies from 0.5 m to 100 m with highest resolution towards the center where the DBHE will be implemented. The different rock types in the structural models are defined by their physical rock properties relevant to solve the heat equations (Table 6 in Supplementary Material S1). Those properties are assigned to every element of the numerical model.

2.1.2 Thermal field around Heat Exchanger at two locations

In all models the temperature at the surface and the temperature at the base of the model are defined by 1st-kind (Dirichlet, **Error! Reference source not found.**) constant value boundary conditions:

Equation 1

$$T_S(\mathrm{x}, t) = T_S^R(t)$$

R denotes the boundary, T_S is the temperature of the solid phase, *x* the Eulerian spatial coordinates and *t* is the time.

An annual average surface temperature is set on all nodes at the top slice. The single node in the center of the model, where the well is located, is excluded to enable free temperature adjustment according to the BHE. In nature, the temperature of the groundwater level responds to the seasonal changes of air temperature, while the groundwater below 10 m to 20 m is usually unaffected. It is therefore reasonable to neglect seasonal changes in the model and assume the annual mean air temperature for the groundwater surface. For the investigated region, the German meteorological service provides an annual mean temperature of 9.8 °C for the location of the NS well and 9.4 °C for the SD well.

The assumed temperature at the model bases is set using the GeotIS thermal model (Agemar et al. 2012). Based on this, a constant temperature of 152 °C at 5.000 m below mean sea level is assumed for the NS well and 164 °C for the SD well. As the NS model extends to a total depth of 5.5 km, the temperature at the base of the model was linearely extrapolated to 166.148 °C (dotted line in **Error! Reference source not found.** and **Error! Reference source not found.**).

In FEFLOW the basic equation of the conservation of thermal energy in the subsurface around the BHE comprises an advective and a conductive part and is formulated in (Diersch 2013) as follows:

Equation 2

$$H_s = \frac{\partial}{\partial_t}[(n\rho^f c^f + (1-n)\cdot\rho^s c^s)\cdot T_s] + \nabla(\rho^f c^f \boldsymbol{q} T_s) - \nabla(\Lambda \cdot \nabla T_s)$$

Where t is the time, n is the porosity, ρ is the density of the fluid (superscript *f*) and the solid phase (superscript *s*) and c is the heat capacity. $\boldsymbol{q}$ is the vector of the volumetric Darcy flow, which is here set close to zero, to simulate only the conductive heat transport in the rock surrounding the BHE. The advective part of the equation is therefore tending to zero. The Λ is the tensor of hydrodynamic thermodispersion (details in Diersch 2013). H_s represents a heat source due to radiogenic heat production of the rocks.

The initial thermal field is determined by a steady-state purely conductive calculation of the heat transport without consideration of the borehole heat exchanger. The results are two thermal fields, which represent the equilibrium temperature distribution after an infinite amount of time according to the material properties (green lines in Figure 3 and Figure 4). The hydraulic processes are to be neglected in a consolidated rock environment as we simulate a closed loop system without any pumping or injection activity. The material properties relevant to the hydraulic calculation, namely the k_f-values for each spatial direction, are therefore set to very small values to prevent fluid flow.

Calculation of initial conditions was done for each model separately and for each scenario with variable material and/or boundary conditions. The initial thermal field along the BHE down to the total model depth for the base cases of the SD and NS wells are visualized with a green line in **Error! Reference source not found.** and in **Error! Reference source not found.**, respectively.

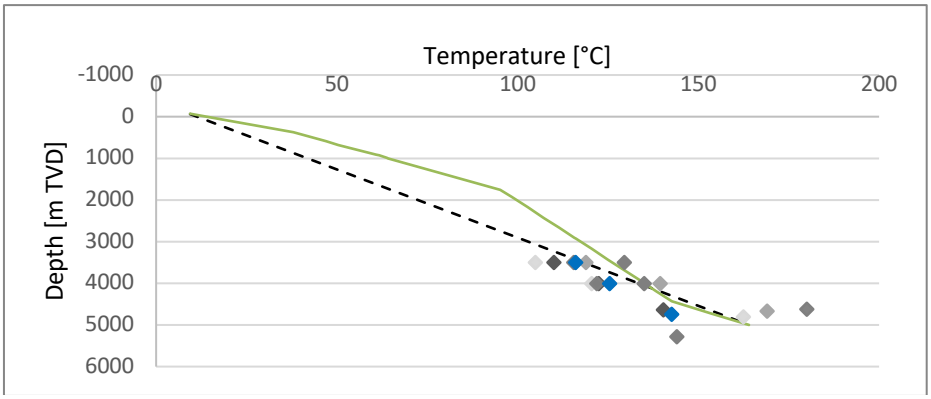

Figure 3: Temperature measurements in grey from different wells in the vicinity of the SD well location and in blue from the SD well location. In dotted black the linear gradient from GeotIS data base and in green the simulated inital thermal field.

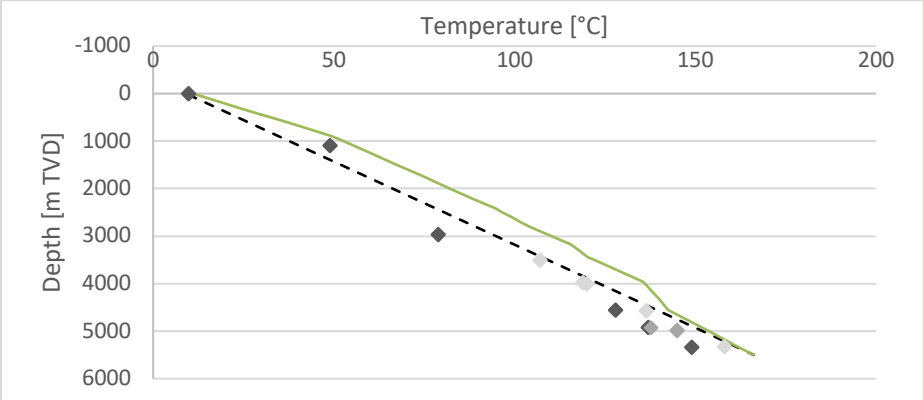

Figure 4: NS well location temperature measurements from BHT (bottom hole temperatures) in medium grey, from MRT in dark grey and from other unknown measurements in light grey. The linear thermal gradient from GeotIS data base is illustrated with a green line and the calculated initial thermal field with a green line.

2.1.3 Recompletion of idle wells into Deep Borehole Heat Exchanger

In FEFLOW, the BHE is defined as a 1D-element boundary condition on mesh edges along a continuous, vertical mesh line across multiple layers. Processes within the BHE are calculated separately from the finite element model of the surrounding rock. The BHE is embedded in the superordinate finite element model and is coupled to the surrounding rock in each numerical iteration using thermal transfer relationships (Diersch et al. 2011; Diersch 2013), in more detail in Supplementary Material 2.

During simulation, the heat budget for a defined domain can be stored in the FEFLOW output file. In our case of the considered BHE domain has been defined along the mesh nodes containing the boundary condition of the BHE. With FEFLOW, the in and out flow of the model domain is calculated along these nodes in every time step. The extracted energy per time unit via this boundary condition is equal to the thermal power output of the BHE (DHI Wasy). The thermal power P [W] can also be calculated analytically when the injection temperature (T_i) [°C] and output temperature (T_o) [°C] are known. Using pressure and temperature dependent specific heat capacity (c_f) [J/(kg K)] and density (ρ_f) [kg/m³] for water (as used as refrigerant) provides an even more precise estimate of the thermal power:

Equation 3

$$P = \rho_f c_f Q (T_o - T_i)$$

The flow rate Q [m³/s] and the inflow temperature are fixed to a constant value in every executed simulation, while the outflow temperature is calculated for every timestep in the simulation (Brown et al. 2021; Dijkshoorn et al. 2013; Liu et al. 2019).

For this study we parameterized the completion and operation data of the BHE according to existing coaxial DBHE: (1) Weggis (Switzerland; Eugster und Füglister 2001 and Kohl et al. 2002) and (2) Arnsberg (Germany; Le Lous et al. 2015 and Garcin 2016) as shown in Table 1.

Table 1: dimensions and material properties for the completion of the borehole heat exchanger with the operation data for each the Weggis and Arnsberg schemes. Illustration of the dimensions see also Figure 22 in Supplementary Material S2.

Parameter	Injection Temperature	Flow Rate	Borehole Diameter (D)	Inlet Diameter (d_c)	Casing Thickness (c-thickness)	Outlet Diameter (d_t)	Tubing Thickness (t-thickness)	Thermal Conductivity Steel Casing	Thermal Conductivity Tubing	Thermal Conductivity Cement
Unit	[°C]	[m3/d]	[m]	[m]	[m]	[m]	[m]	[W/m/K]	[W/m/K]	[W/m/K]
Weggis	35	146	0.279	0.177	0.01	0.073	0.016	50	0.09	2
Arnsberg	40	264	0.275	0.195	0.01	0.127	0.0536	54	0.15	2

The properties of the refrigerant are are implemented directly in the BHE dataset editor in FEFLOW. They are independent from the reservoir model, as the system of the BHE is completely closed. There are several possible working fluids, which could be circulated in the DBHE. Water is the best refrigerant (Alimonti et al. 2018) and after Stober und Bucher (2020) it has (besides its high density) beneficial properties for use as heat transfer fluid. Moreover, there are several DBHE with water as refrigerant, which have been in operation for years (i.e. Arnsberg, Weggis, Prenzlau). For these reasons, we chose water as refrigerant for the numerical simulations of this study with the following fixed properties: Dynamic viscosity of 1.307 E-03 kg/(m s), density of 999.7 kg/m^3, volumetric heat capacity of 4193.7415 J/(m^3 K) and thermal conductivity of 0.579 W/(m K).

The selection of the production tubing for the DBHE is of central importance for achieving a high production temperature and thus a high thermal output (Michalzik et al. 2010). Besides having to resist high tensile strength and high formation temperature, there are several further requirements that can be summarized as follows: (a) good thermal insulation along the tubing string including connectors, (b) technical reliability

(thermal stability) and corrosion resistance (tightness), (c) low maintenance costs during long-term operation, (d) standard pipe material according to API if possible, (e) standard pipe handling and installation (preferred). Various different options were discussed for this project. There are a few hints in the literature, that the collapse of tubing lead to complications in past DBHE completions; i.e., Aachen Super C well (i.e. Rheinisch-Westfälische Technische Hochschule Aachen (2011), Bundesverband Geothermie (2023)) and Arnsberg glass-fiber reinforced plastic material (GFK) tubing first attempt, Garcin 2016). Besides the successfully installed tubing pipes of Arnsberg and Weggis, after an extensive market research the vacuum insulated tubing (VIT), which was installed this year in the Eden geothermal project seems to be the material of choice with a full insulation across the body and coupling of the pipe results in a thermal conductivity in the order of 0.02 to 0.03 W/ (m K) (Shandong SLOFE Petroleum Machinery).

2.2 Calculation of heat generation costs based on infrastructure simulations

For the calculation of the heat generation costs, the above surface infrastructure needs to be mapped and calculated. Therefore, possible heat consumers were mapped in the vicinity (of several kilometers) around the two well locations, with a focus on public institutions.

2.2.1 Heat demand calculations

The energy demand for hot water and space heating of buildings depends on various factors, such as the building's location, climate, size, occupant behavior, or insulation level. The BDEW standard load profile procedure (Bundesverband der Energie- und Wasserwirtschaft e.V. (BDEW) 2011) is here used to calculate the expected energy consumption.

To estimate the annual energy demands for heating, the average consumption for each building is determined based on the AG Energiebilanzen e.V. (AGEB) application balances (Geiger et al. 2019). The AGEB application provides balances for the commercial, trade, and service sectors. AGEB provides the annual energy consumption of various business types depending on a suitable reference unit, for instance, hospital beds for hospitals, employees for office buildings, or students for schools.

The weather conditions for the demand calculations are derived from the Test Reference Year (TRY) of the Deutscher Wetterdienst (Deutscher Wetterdienst (DWD), Bundesamt für Bauwesen und Raumordnung (BBR) 2017) and describe a representative course of outside temperature, wind conditions, and solar radiation depending on a selected location.

2.2.1 Techno-Economic Simulation of the Transport Grid

Generally, a thermal grid consists of consumers, pipes, pumps, transfer stations, and production units. All those components have operational expenditures (opex) and capital expenditures (capex). The economic calculation is based on the VDI2067 norm . The investments $capex^{\text{technology}}$ are discounted on a time horizon $t^{\text{horizon}} = 10\ a$ with a discount rate of $\omega = 6\ \%$, resulting in an annuity factor of 0.136 and a bar value factor of 9.434. Every technology has a lifetime t^{lifetime} and their remaining value after ten years is calculated with:

Equation 4

$$capex^{\text{technology}} = \frac{t^{\text{lifetime}} - t^{\text{horizon}}}{t^{\text{lifetime}}(1+\omega)^{t^{\text{horizon}}}}.$$

The investments are multiplied by the annuity factor, and the opex are multiplied by the bar value factor and the annuity factor.

The most significant economic impacts are caused by the investments in the production units and the heat grid. The transport from the production unit to the consumers via pipes causes thermal losses, which are simulated based on Glück (1985)

Equation 5

$$T^{\text{out}} = T^{\text{soil}} + \left(T^{\text{in}} - T^{\text{soil}}\right) e^{-\frac{U\pi dl}{c_{\text{p}}\dot{m}}}.$$

Here T^{in} and T^{out} are the injection and extraction temperatures inside a pipe of the grid, T^{soil} is the soil temperature, U is the heat transfer coefficient depending on the pipe's insulation – a value of 1.2 W/(m^2 K) was assumed in this study. d, l, and $\dot{m}$ are the pipe's diameter, length, and mass flow, respectively. The specific heat capacity of water is denoted by c_{p} – in this study, set to a value of 4230 J/(kg K). Increasing the length of the pipe causes higher losses and a lower extraction temperature. Based on Sporleder et al. (2022), most simulations work with temperatures above 60 °C at the consumer's transfer station. Therefore, we set the technical potential to $T^{\text{out}} \geq 60$ °C for $T^{\text{soil}} = -10$ °C. The diameter of the pipe depends on the transported heat $\dot{Q}$ and the allowed pressure losses. We assumed a maximum pressure loss of 200 Pa/m (Verenum 2017). We calculated the diameter and flow rate based on the Darcy-Weißbach Equation and the transported heat, assuming a temperature delta between the forward and backward pipe of 30 K.

The investment of the pipe depends on the diameter, the length, and the structure of the ground. The specific investments are calculated based on Steinbach et al. (2020) with

Equation 6

$$c^{\text{invest}} = 0.1692\dot{Q} + 392.69.$$

The lifetime of the pipes is set as 30 years. The opex of the grid are caused by the pumps circulating the water. A specific value of 0.0012 €/kWh is assumed (Steinbach et al. 2020).

The next component is the production unit – here, the geothermal well. The investments are assumed to be 1 Mio. € for the SD well and 1.25 Mio. € for the NS well location, based on a rough technical estimation for recompletion costs of the two wells. The opex are accounted as fixed with 58 €/kW based on Steinbach et al. (2020) for deep geothermal energy units. The lifetime of the component is 30 years, and the efficiency of the BHE on the surface is 96 %. The transfer station at the well also has a lifetime of 30 years and a specific investment value of 64 €/kW. The pump station has a lifetime of 20 years and specific investments of 60 €/kW. The transfer station at the consumer has a lifetime of 30 years, an efficiency of 96 %, and specific investments of 26.17 €/kW. (Steinbach et al. 2020) The specific investments for the transfer station at the production unit is higher because of additional equipment (BHE, pipes) to transport the heat from the well extraction point to the grid. Finally, we calculate the heat generation costs by dividing the total costs – opex and capex – by the consumed heat.

2.3 Sensitivity Analysis

In development and evaluation of numerical models, understanding how strongly the variation of model parameters impacts model prediction is essential. One methodological approach to this is sensitivity analysis, for identifying the influence of model parameters on the model (Degen et al. 2021), and in a wider context to study how uncertainty in model input parameters propagates to uncertainty in model predictions (Linda Lilburne und Stefano Tarantola 2009). In principle, sensitivity analysis can be classified by its framework (deterministic versus stochastic) and whether it is carried out locally or globally (Sobol′ 2001).

Local sensitivity analyses are used to determine the impact of model parameter changes on the model results in relation to a set of reference parameters (Wainwright et al. 2014), i.e. a so-called “base case”. Definition of such a set of reference parameters thereby already influences the sensitivity analysis. In addition, local sensitivity analyses do not consider correlations between parameters (Degen et al. 2021). Global sensitivity analysis, on the other hand, evaluates the influence of model parameters without the need of defining a reference set. Different approaches exist, such as the Sobol sensitivity analysis (Sobol′ 2001), which evaluate the whole parameter space within pre-defined ranges and assess parameter correlations. While thorough in terms of identifying sensitivities which may not be in the vicinity of a “base case” parametricly, these methods are often demanding as they require a lot of forward models. Thus, they usually depend on approaches like surrogate models to compensate high computational costs (Degen et al. 2021).

In this study, we chose a local sensitivity analysis approach and vary different paramters relative to a pre-defined “base case” set. We divide the variations in parameters above- and below surface and parameters of the DBHE:

- Parameter variation of above surface: distance between consumer and heat source and yearly operation hours of the DBHE
- Parameters of subsurface: thermal gradient, thermal conductivity of salt diapir

- Parameters of DBHE: recompletion depth, tubing material, well diameter, flow rate and injection temperature

3 Results

The heat source is as relevant as the heat grid for a successful heat supply from geothermal energy. Therefore, this study comprises both the simulation and prediction of the subsurface heat source of the deep borehole heat exchanger (Section 3.1) as well as the above surface infrastructure consisting of the heat demand mapping and the calculation of the heat generation costs (Section 3.2).

3.1 Subsurface Results for the Prediction of Thermal Power

Conceptually, the BHE simulation results can be applied to all deep gas wells in the NGB. Therefore, a list of parameter variations was catalogued, including all parameter combinations based on the realistic sum of all idle wells from ExxonMobil Production Deutschland GmbH. The scenarios include realistic operating parameters for: (1) flow rate and (2) injection temperature, geological uncertainties: (3) thermal conductivity of the Zechstein salt, and (4) variations in the temperature gradient and a range of recompletion parameters: (5) maximal completion depth of the BHE, (6) well diameter and (7) tubing material (Figure 5). The tested parameter ranges are illustrated in Figure 5 and represent the geological uncertainties and realizable operation values.

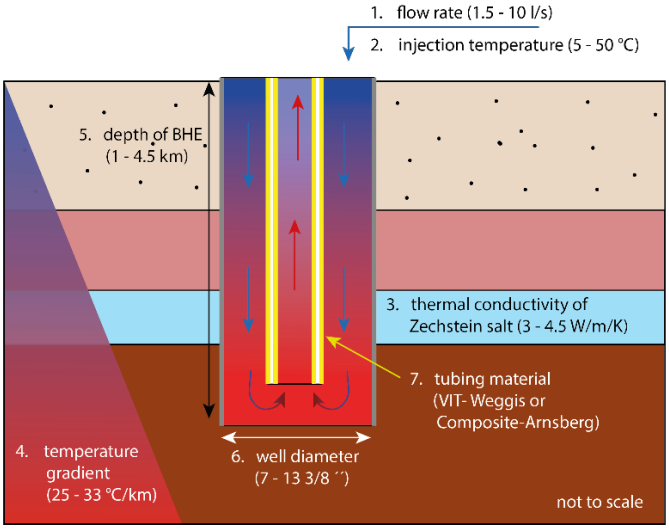

Figure 5: Overview of parameter ranges for the sensitivity analysis to predict the thermal power of the deep borehole heat exchanger independent of the exact location and well dimensions.

We formulated base case scenarios to compare the predictions with already installed DBHE, which are the basic simulations for the parameter sensitivity studies. The base

cases compensate the two different geological setting as introduced in Section 1.2. NS for a well through a normal stratigraphic setting for the NGB and SD representing wells through a salt diapir. Combining these two exemplary locations with completion and operation parameters of two different active deep BHE (Table 1), namely Weggis (Switzerland) and Arnsberg (Germany) leads to four base cases for our simulations:

1. Base case 1 is the normal stratigraphic setting with the completion scheme and operation parameters of the Weggis heat exchanger (NS Weggis)
2. Base case 2 is the normal stratigraphic setting with the completion scheme and operation parameters of the Arnsberg heat exchanger (NS Arnsberg)
3. Base case 3 is the salt diapir geology with the completion scheme and operation parameters of the Weggis heat exchanger (SD Weggis)
4. Base case 4 is the salt diapir geology with the completion scheme and operation parameters of the Arnsberg heat exchanger (SD Arnsberg)

Table 2 presents a comparable overview on the calculated thermal output of the four base cases. In the NS well location the total thermal output is predicted to be higher with 294 kW and 376 kW depending on the re-completion scheme of Weggis and Arnsberg respectively, than the thermal output for the SD well location with 241 kW and 287 kW respectively. The thermal output per meterage on the other hand is higher for the BHE through a thick salt layer (in base case 3 and 4) with 86 W/m and 102.5 W/m respectively than in the normal stratigraphic setting with 68 W/m and 87.4 W/m.

Table 2 input parameters and thermal output of the BHE for the four base cases. Bold values are the input parameters for the heat grid simulations to calculate the heat generation costs.

	Base case 1 NS Weggis	Base case 2 NS Arnsberg	Base case 3 SD Weggis	Base Case 4 SD Arnsberg
Total depth [m]	4.3	4.3	2.8	2.8
Temperature at total depth [°C]	139	139	114	114
Injection temperature T_i [°C]	35	40	35	40
Flow rate Q [l/s]	1.7	3.1	1.7	3.1
Production temperature after 5 years of operation time T_o [°C]	78	72.2	69.2	64
Production temperature after 30 years of operation time T_o [°C]	**74**	**68.7**	**66.6**	**61.7**

Heat extraction rate after 5 years of operation time P [kW]	313	417	258	317
Heat extraction rate after 30 years of operation time P [kW]	**294**	**376**	**241**	**287**
Heat extraction rates per meterage after 5 years [W/m]	73	97	92	113
Heat extraction rates per meterage after 30 years [W/m]	68	87.4	86	102.5

3.1.1 Sensititivy Testing

Originating from the four base cases (Section 3.1), 220 model scenarios were run to evaluate the sensitivities of the geological uncertainties, the well dimensions, the completion schemes, and the operating parameters on the calculated thermal output of the deep BHE. With tornado charts, we present the impact of the different parameters on each base case. With this visualization it is only possible to show one time step of the predicted thermal power, in Figure 6, Figure 7, Figure 8 and Figure 9 we decided as a base of comparison, to show here the thermal output after 30 years of operation time. When the DBHE is not in steady-state conditions with the surrounding rocks, a decreasing thermal output over 30 years of operation can typically be observed in all scenarios. To describe the minimal thermal output, we focus on the values after 30 years of operation time in this study. When the installation would be optimized according to the heat supply and heat demand, it would be important to minimize the total decrease over time to ensure a constant heat extraction rate for 30 years and longer.

Minimal and maximal values of the bars represent the tested range of this parameter sensitivity study. The parameter with the highest impact is the uppermost bar, followed by decreasing importance downward. It is important to note that this is only a local sensitivity study, where all base case parameters are constant and only one parameter is varied in the scenarios between the min and max values (Wainwright et al. 2014). As the choice of min and max values heavily influence the sensitivity analysis, we chose to set physical and geological meaningful values and operation values in the range of comparable applications. A global sensitivity study would improve the understanding of parameter correlations and would be necessary for optimizing the installation. This study focuses on the complete system including grid, well, and consumer.

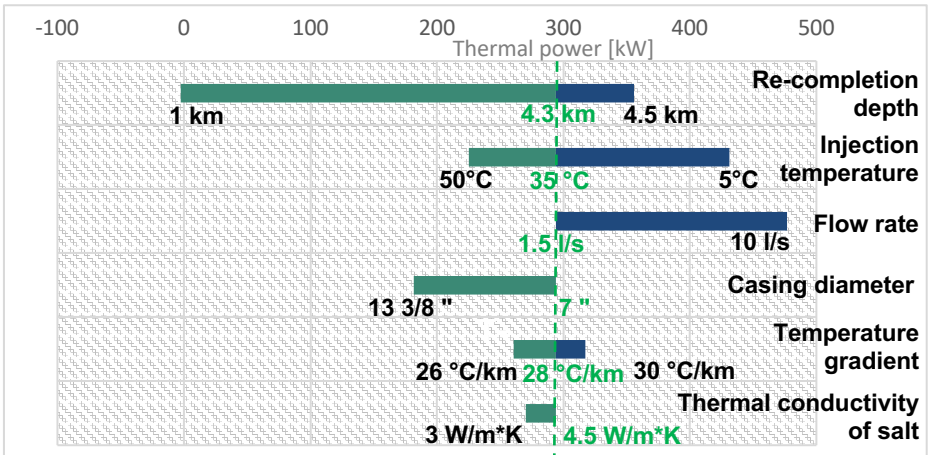

Figure 6: Results of base case 1 NS Weggis (294 kW), after 30 years of operation time visualized in a tornado chart. This chart shows results from minimum, maximum and base case parameter values.

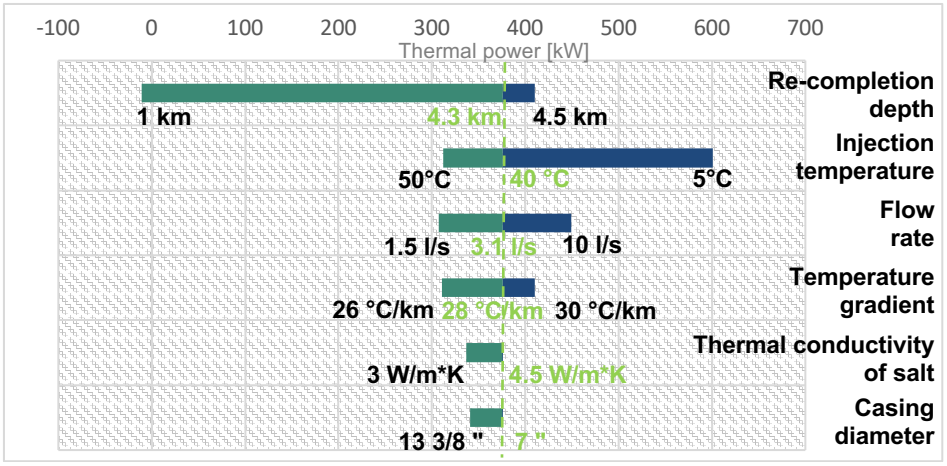

Figure 7: Results of base case 2 NS Arnsberg (376 kW), after 30 years of operation time visualized in a tornado chart. This chart shows results from minimum, maximum and base case parameter values.

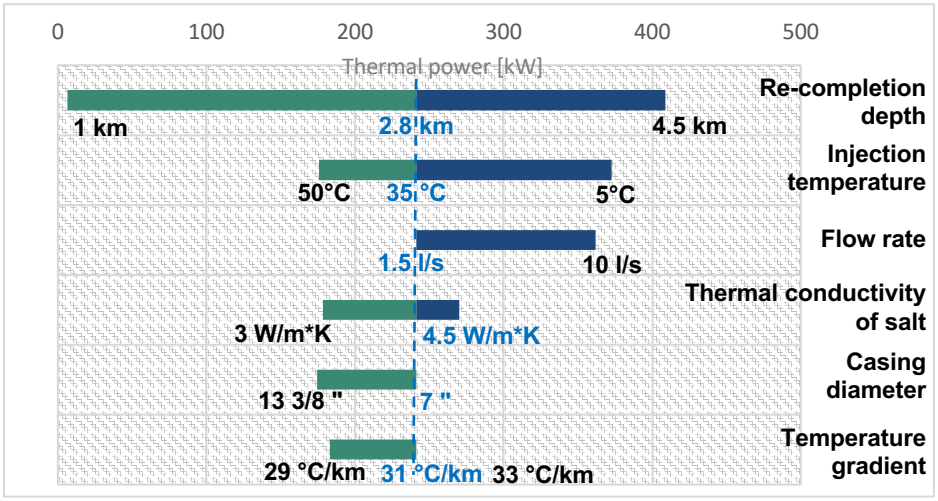

Figure 8: Results of base case 3 SD Weggis (241 kW), after 30 years of operation time visualized in a tornado chart. This chart shows results from minimum, maximum and base case parameter values.

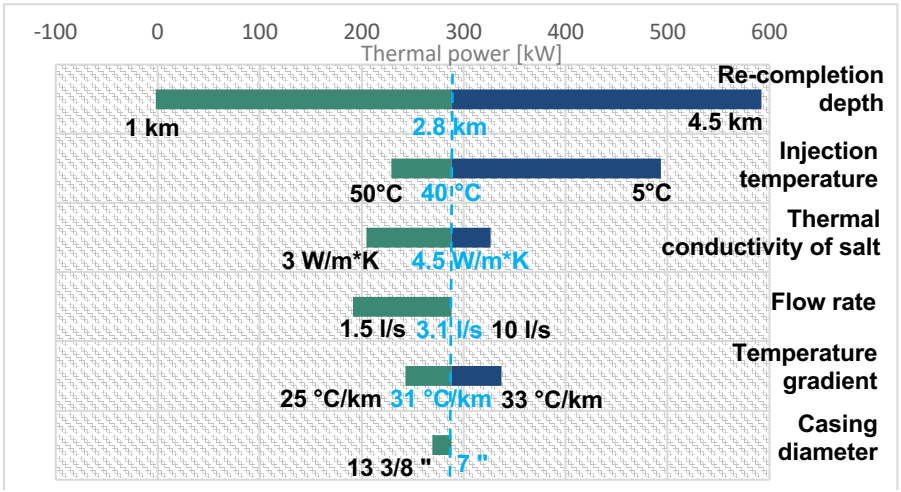

Figure 9: Results of base case 4 SD Arnsberg (287 kW), after 30 years of operation time visualized in a tornado chart. This chart shows results from minimum, maximum and base case parameter values.

Results show that the re-completion depth has the highest impact on the calculated thermal output in all base cases. The tested range was between 1 km depth and 4.5 km depth. In base cases 1 and 2 (Figure 6 and Figure 7), the re-completion depth is already near the maximum value; therefore the optimization possibility is lower than in base

cases 3 and 4 (Figure 8 and Figure 9), where the re-completion depth of the well is only 2.8 km. Worth mentioning is the fact that in base cases 1, 2 and 4, the re-completion depth of only 1 km leads to negative thermal power. This negative thermal power is caused by higher injection temperatures than the temperature of the surrounding rocks. In base case 3, higher geothermal gradient and lower injection temperature in combination lead to very small but at least positive thermal power in the scenario with a re-completion depth of 1 km. In the four base cases, very high reinjection temperatures of 35 °C and 40 °C are set (Figure 6, Figure 7, Figure 8 and Figure 9). Reducing the injection temperature (T_i) increases the thermal power, but reduces the production temperature (T_o) and has thereby a negative effect on the quality of the heat source (further discussed in Section 4).

The flow rate is the second operation parameter, which can be optimized while the BHE is active. In general, it can be stated that reducing the flow rate leads to higher pumping temperatures but lower thermal output. On the contrary the thermal power can be maximized with higher flow rate but concurrently, the production temperature is cooled down. The flow rate has a medium high impact on the total thermal output of the DBHE. An increase of the flow rate leads to higher calculated thermal power. That This effect is most sensitive in base cases 1 and 3, where the flow rate is very low with 1.5 l/s. In base cases 1, 2 and 3 the flow rate is the third most important parameter, in base case 4, on the fourth position. In contrast to the re-completion depth, the injection temperature, the geothermal gradient, and the thermal conductivity of the salt, the flow rate is not linearly correlated with the thermal output. Therefore, in the plot of flow rate against thermal power (Figure 10) the correlation after 30 years of operation time is visualized. For very low flow rates of 1.5 l/s the calculated thermal output is almost equal, independent of the installation (Weggis or Arnsberg). The results lead to the conclusion that the thermal outputs of DBHEs operating with very low flow rates are nearly independent of the re-completion scheme and the injection temperature. But as both parameters re-completion scheme and injection temperature are changed, it could be a higher-order correlation effect, too. This is shown in Figure 10 comparing base case 1 against 2 and base case 3 against 4, the two green and the two blue curves overlap between 1.5 and 3.1 l/s of flow rates and the spreading occurs only with higher flow rates. Overall, thermal power yields in the SD well location (blue) are lower. However, looking at re-completion schemes, the higher the flow rate is, the higher is the difference between the Weggis installation (base cases 1 and 3) compared to the Arnsberg installation (base cases 2 and 4). The configuration of the different tubing as well as the different injection temperatures affect these scenarios.

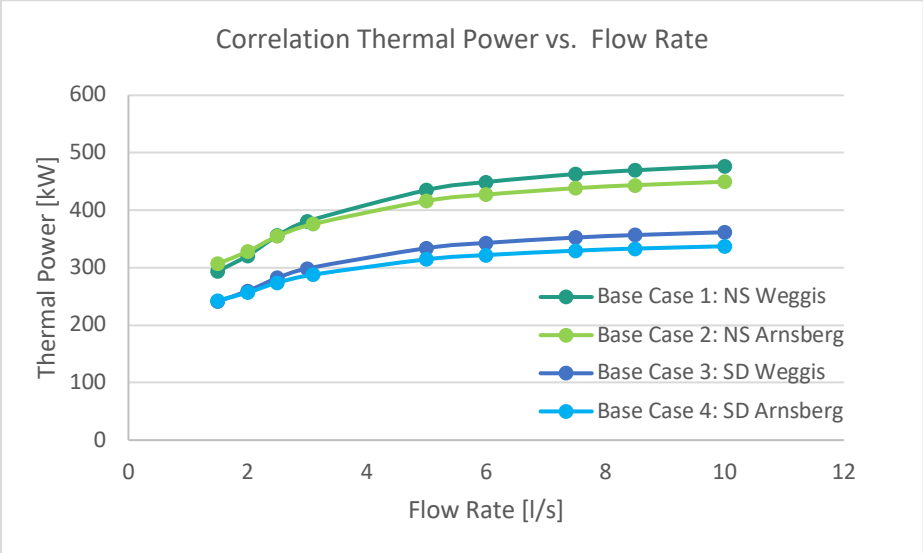

Figure 10 Flow rate scenarios of all four base cases. Illustrated in green for the NS well location and in blue for the SD location.

The thermal power is mainly increased between a flow rate of 1.5 and 5 l/s. Flow rates above 5 lead only to a minimal increase of the thermal power output. In base case 1, flow rates between 1.5 and 5 l/s lead to an increase of thermal power of about 77 % (total difference of 141 kW) after 30 years of operation time and between 5 l/s and 10 l/s, the thermal power output is only further increased by 23 % (total difference of 42 kW, Figure 11). The spreading of the scenario results is decreasing with operation time in all base cases and is lowest after 30 years (Figure 11). In all scenarios and base cases, the thermal power output is decreasing with operation time of the DBHE.

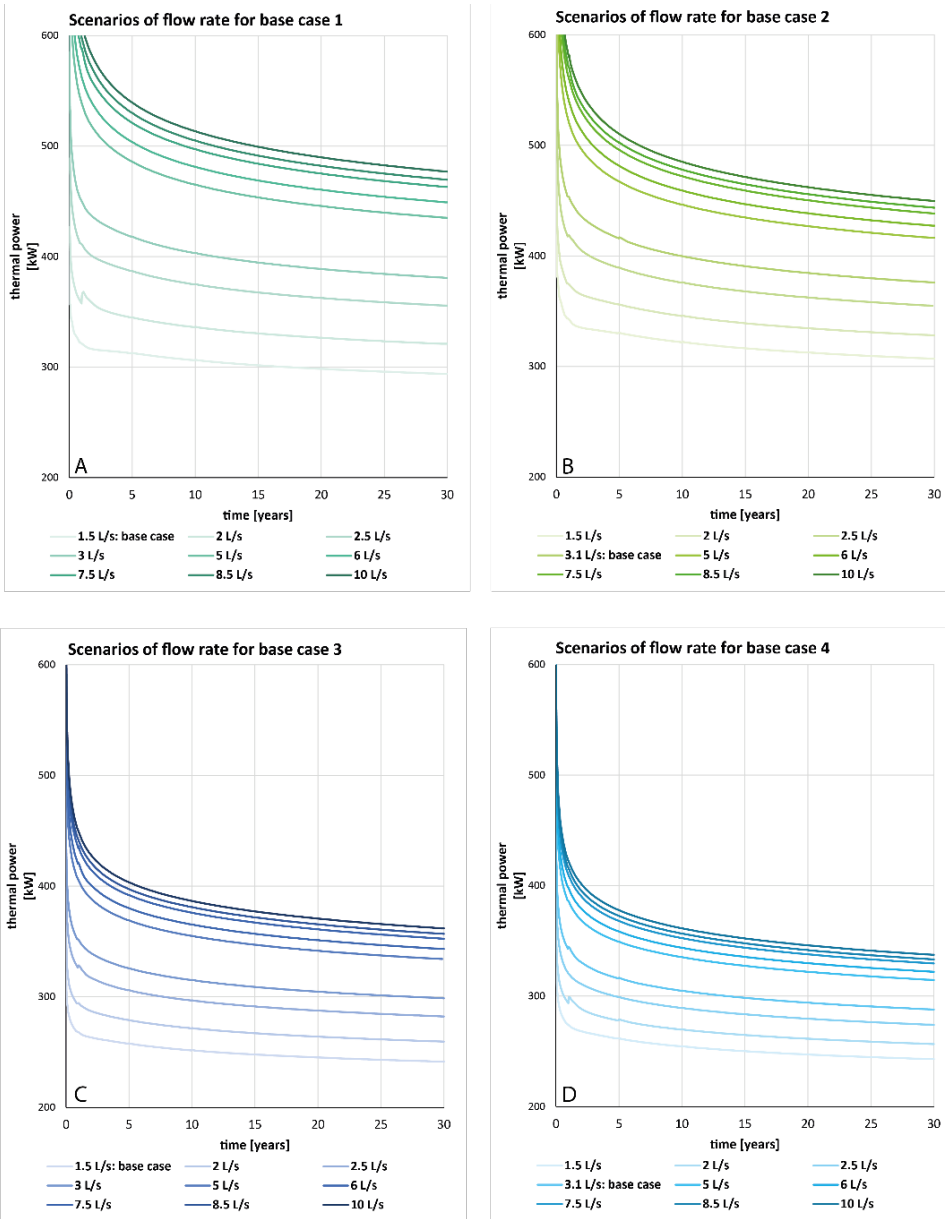

Figure 11 Four base cases with scenarios of variable flow rate: (A) Base case 1 NS Weggis, (B) Base case 2 NS Arnsberg, (C) Base case 3 SD Weggis and (D) Base case 4 SD Arnsberg. Thermal power reduces with time in all base cases and all scenarios. Highest values of thermal power in the first 2 years above 600 kW are neglected to better visualize the long-term evolvement. In the first days of production, the thermal power is predicted to be higher than 1 MW.

The first two base cases in the normal stratigraphic setting (NS) show clearly that the importance of the thermal conductivity is very low. This effect can be explained by

the thinner Zechstein salt layer, when compared to the salt dome (SD) scenarios. There, in base cases 3 and 4, the thermal conductivity in the Zechstein salt diapir plays an important role and affects the thermal power output (Figure 8 and Figure 9). The uncertainty of the thermal gradient is rather low in the simulations, as there is a very good data basis as temperatures measurements in high depths are included in the model (**Error! Reference source not found.** and **Error! Reference source not found.**). But we still see the impact of the initial thermal field in the simulation results in all tornado charts.

The last parameter is the thickness of the casing. In all base cases we observe a negative impact of higher casing diameter. This might be an effect of the tubing size, which was adjusted simultaneously. The fluid is cooled down, when its pumped up, and this leads to reduced thermal output. The minimal higher heat transfer surface between the casing and the surrounding rock in the scenarios with casing thicknesses of 9 5/8´´ and 13 3/8´´ is not high enough to compensate for the higher tubing thickness.

3.1.2 Reservoir temperature and cooling effects around the well

The heat exploitation of the subsurface is accompanied by a gradual cooling in the near field of the borehole, which acts as a heat sink (Figure 12Figure 13) over time. The spatial, horizontal temperature distribution for a given time step within the operation time is expected to decrease in a concentric way around the BHE, given a horizontal homogeneity of the host rock. As shown in Figure 12, with ongoing operation time, the radius influenced by the heat extraction increases.

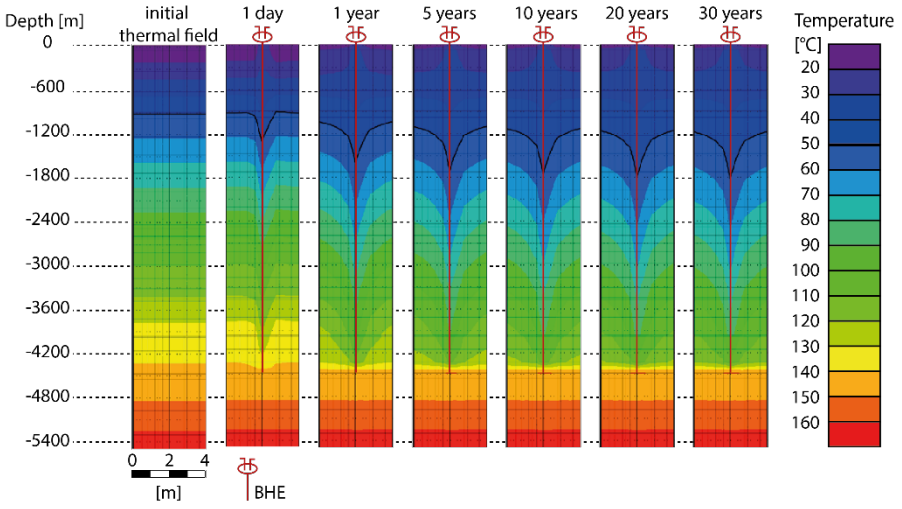

Figure 12: Development of a cone of reduced temperatures in the near field of 2 m around the DBHE in base case 1 with increasing operation time from the left (initial state) to the right (after 30 years).

In Figure 13, the thermal field of the model of base case 1 in a horizontal slice in 3 km depth is shown. The initial temperature is 109 °C at this depth. The 100 °C isotherm propagated 3 m (very light green) from the heat sink after one year of operation time. After 10 years, it propagated to a distance of about 6.5 m, after 20 years to about 9 m and after 30 years to about 11 m (dark green line in Figure 13). The propagation of the 90 °C isotherm (indicated with blue lines and a blue arrow in Figure 13) is also after 30 years only a few meters away from the BHE.

The propagation of the isotherms is not constant over operation time. The cooling effect is highest in the first five years of operation and is reduced gradually over the period of heat extraction (Figure 13). Given a continuous influx of heat to the geological system, the existence of a state of equilibrium regarding the temperature distribution and heat flows is assumed. The amount and speed of the cooling propagation and the state of equilibrium depend on the amount of extracted heat and surrounding rock parameters.Moreover the results show after 30 years of operation time only 10 % temperature decrease in a distance of 10 m afound the BHE. Similar to other BHE this results shows that DBHEs could also be installed in fields with multiple idle wells.

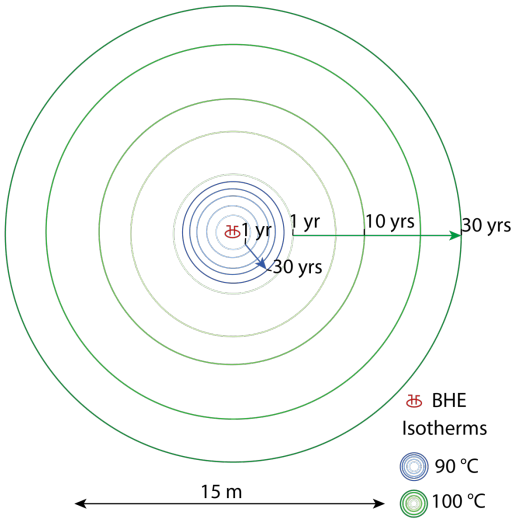

Figure 13: Propagation of the 90 °C and 100 °C isotherms with increasing operation time of 1 year, 5 years, 10 years, 20 years and 30 years from light to dark colors. The isotherms are extracted at a horizontal slice in 3 km depth were the initial temperature is 109 °C in this base case 1. Green lines indicate 9 °C cooling in the surrounding of up to 10 m around the borehole after 30 years of operation time. The 90 °C isotherm (in blue) so cooling of about 19 °C propagates only few meters in 30 years of operation.

3.2 Surface infrastructure modelling of the district heating system

Before the economic analysis of the location, including the simulation of the heat grid, is possible, heat consumers in the region around the drilling locations were identified with application examples and system concepts. The district heating system

design included the efficiency and economic viability of the overall system as a function of distance, subsurface parameters and customer structures.

3.2.1 Heat demand mapping for the two well locations

For the borehole location of the normal stratigraphic setting (NS well location), four public buildings representative for a typical north German community were chosen to be hypothetically located in close proximity to the wells: A kindergarden, two different normal sized schools (which differ in number of pupils) and a swimming pool. Before applying the standard load profile procedure, the annual energy demands for heating and hot water were determined using open data of the selected buildings and data for the typical energy consumption of the specific buildings types from Geiger et al. (2019). With the specific energy demands per reference unit, in MWh/RefU, the resulting total energy demands in MWh for heating and hot water are calculated and shown in Table 3. The resulting demand load profiles are shown in Figure 14.

Table 3: Overview of estimated building data for the demand calculation of selected buildings for the NS wellbore location, for base cases 1 and 2.

	Specific annual heat demand [MWh/RefU]	Total annual heat demand [MWh]
Kindergarden	1.13	101
School 1	1.13	395
School 2	1.13	225
Swimming Bath	0.61	368

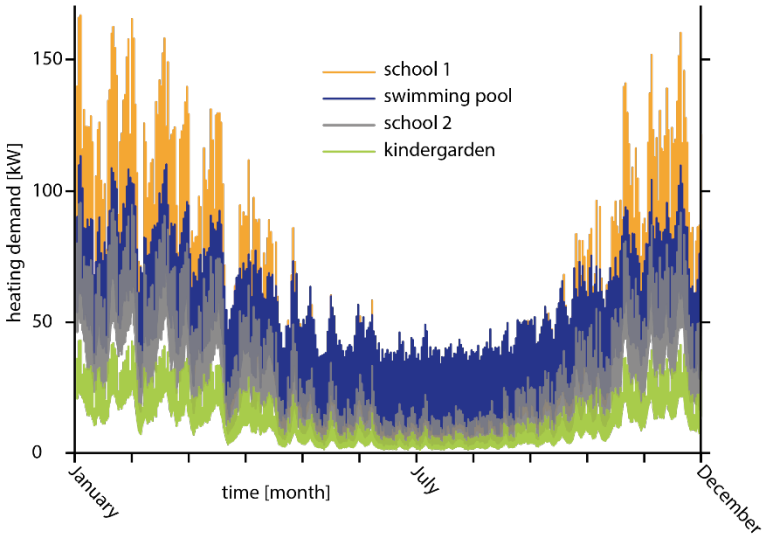

Figure 14: Resulting heat load profiles of selected buildings for the NS borehole location based on the standard load profile procedure. In green: kindergarden, blue: swimming pool and in orange: school 1, grey: school 2.

In the vicinity of the wellbore location of the salt diapir well (SD well), four commercial or public buildings were chosen: A mid-sized German hospital, two hotels and a school. The specific annual energy demands for heating and hot water per reference unit were taken from Geiger et al. (2019) and scaled according to the assumed buildings. The results are listed in 4. The resulting heat demand profiles that were calculated with the standard load profile procedure are shown in Figure 15.

Table 4: Overview of estimated building data for the demand calculation of selected buildings for the location of wellbore SD.

Building	Specific annual heat demand [MWh/RefU]	Total annual heat demand [MWh]
Hospital	16.98	6317
Larger-sized hotel	17.44	1325
Small-sized hotel	17.44	558
School	1.13	2254

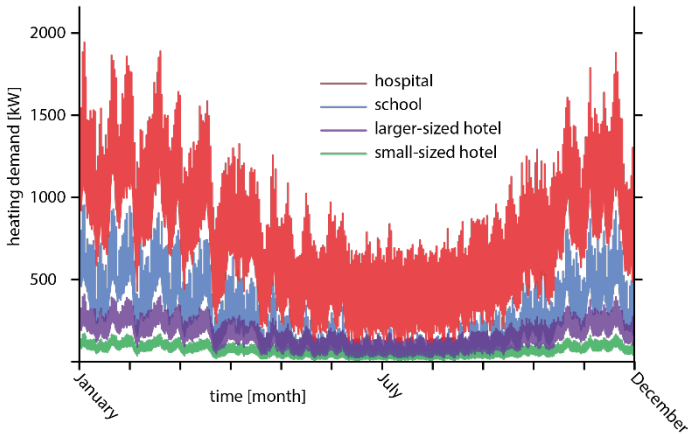

Figure 15: Resulting heat load profiles of selected buildings for the SD borehole location based on the standard load profile procedure. Red: hospital, blue: school, purple: larger-sized hotel and in green: a typical small-sized hotel.

3.2.2 Techno-Economic Analysis of the four base cases

The simulation results, 200 kW to 400 kW thermal output and production temperatures, between 64 °C and 78 °C, are used for the economic calculation of heat generation costs at the well top and for consumers including the heating network.

In Section 2.2.1, the method for the calculations is explained. This method is applied to the four base cases (see Table 2). Every case is reviewed concerning different distances from the well to a set of hypothetical consumers. Even though real locations with potential consumers are considered in this study, we examine the influence of distance on the heat generation costs.

In the first base case, we use a heat extraction rate of 294 kW as the starting value for the techno-economic calculation and an extraction temperature from the well of 74 °C, which are the results of the BHE simulations after 30 years of operation time. Accessible consumers around the NS well location would be at a distance of 2 km to 3 km. Some consumer profiles have been analyzed in section 3.2.1. The results of the heat generation costs, including the grid infrastructure, is summarized in Figure 16.

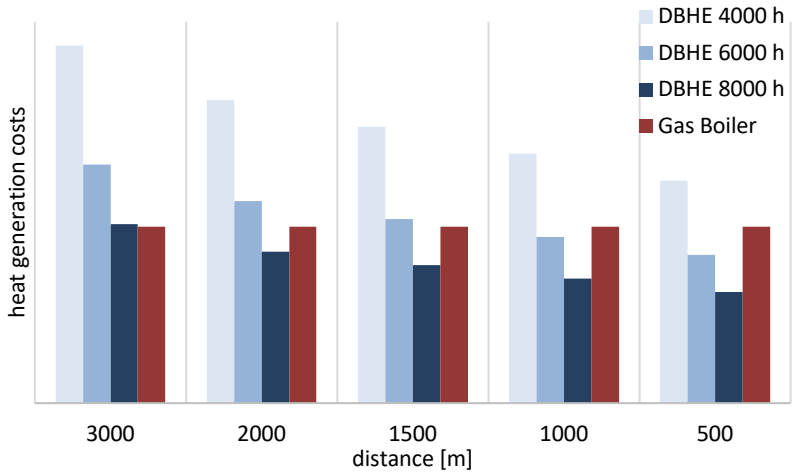

Figure 16: Heat generation costs for different operating hours and a gas boiler as a benchmark for base case 1; the heat generation costs for the DBHE are dependent on the distance to the consumer and the operation hours (increasing from light blue with 4000 h per year to dark blue with 8000 hours per year) of the DBHE.

Figure 16 relates the different heat generation costs depending on the transport distance to each other (from 500 m on the righthand side of the plot to a 3 km distance on the left-hand side of the plot). The technical potential for this scenario is at 10 km distance, meaning the maximal theoretical distance of a consumer to the BHE heat source where a minimum of 60 °C could be delivered is 10 km. For a distance of 3 km and operating hours of 8000, the heat generation costs of the BHE is close to the heat generation costs of the gas boiler. Decreasing the operating hours by half (to 4000 h) results in a doubling of heat generation costs. With 4000 hours of operating time and a distance of 500 m, the BHE is still more expensive than the benchmark. For a distance of 1500 m and operating hours of 6000, the BHE is close to the benchmark and is less expensive for a distance of 1000 m.

The base case 2, the calculations are done with an extraction temperature at the well top of 68.7 °C and a thermal power of 376 kW. In Figure 17, the heat generation costs decrease due to the higher heat flow from the DBHE compared to base case 1. The heat generation costs for the heat exchanger with 8000 hours of operation are below the benchmark at a distance of 3 km. For a distance of 2 km, the BHE with 6000 h becomes less expensive than the gas boiler.

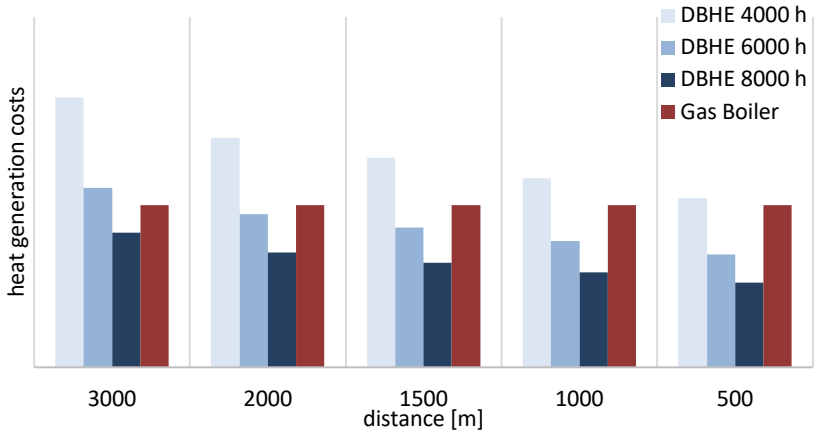

Figure 17: Heat generation costs for different operating hours and a gas boiler as a benchmark for base case 2; the heat generation costs for the DBHE depend on the distance to the consumer (increasing from light blue with 4000 h per year to dark blue with 8000 hours per year).

The distance to an accessible consumer in base cases 3 and 4 is similar to base cases 1 and 2 with 2-3 km. For the third base case, heat generation costs are calculated based on an extraction temperature of 66.6 °C and a heat rate of 241 kW. The technical potential is lower than for base case 1 with 5 km, as the output temperature is also 8 °C lower. Figure 18 illustrates the results for the third base case. Due to the lower heat rate, the heat generation costs are higher, and the DBHE with 8000 operating hours is close to the benchmark for a distance of only 2 km. The DBHE running 6000 h has the same heat generation costs as the benchmark for a distance of 1 km. The heat generation costs are higher than the benchmark for all other operating hours and distances.

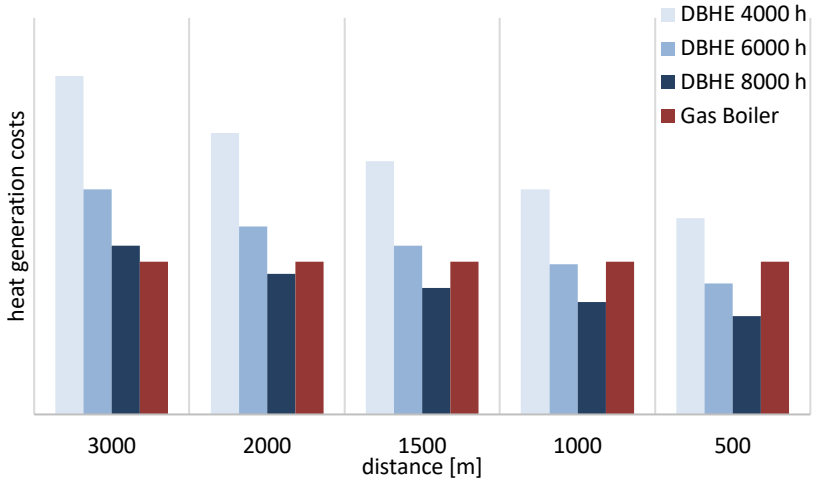

Figure 18: Heat generation costs for different operating hours and a gas boiler as a benchmark for base case 3; the heat generation costs for the DBHE are dependent on the distance to

the consumer; (increasing from light blue with 4000 h per year to dark blue with 8000 hours per year).

Base case 4 operates on an extraction temperature at the wellhead of 61.7 °C with a heat extraction rate of 287 kW. The heat generation costs at the wellhead for the fourth base case are slightly lower compared to the third base case, due to the higher thermal output. The higher thermal power causes a lower production temperature, yielding a lower technical potential of 1500 m. As Figure 19 shows, the costs for a DBHE operating for 8000 h at a distance of 3000 m is below the benchmark. However, for this scenario, the temperature at the consumer would be 58.6 °C and below the technical potential. At a distance of 1.5 km, the calculated heat generation costs of the DBHE running 6000 h are below the benchmark and the heat generation costs of the DBHE running 4000 h are 30 % higher than the costs of the benchmark.

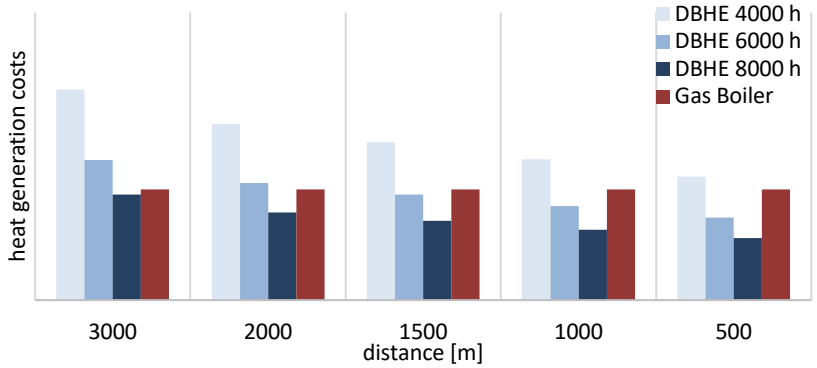

Figure 19: Heat generation costs for different operating hours and a gas boiler as a benchmark for base case 4; the heat generation costs for the DBHE are dependent on the distance to the consumer.

4 Discussion

In this study, we showed that, under certain conditions, borehole heat exchangers in idle wells in the North German Basin can be economically competitive with heat generation costs compared to gas boilers. This result is based on a comparison with existing DBHE installations for two typical geological scenarios and several use cases – even though the estimated thermal power per unit length is lower than estimated in previous studies. According to the Bundesverband Geothermie, it is possible to extract 150 W/m – 250 W/m from a DBHE (Bundesverband Geothermie), which would result in 300 kW – 500 kW for wells with a total length of 2 km and 600 kW – 1 MW for 4 km long wells. With our detailed models of the normal stratigraphic setting location (NS) and the salt diapir setting (SD), we simulated the heat extraction and determined lower values of 86 (base case 3) to 102.5 (base case 4) W/m for the SD location, and even lower values of 68 (base case 1) to 87.4 (base case 2) W/m for the NS location after 30 years of operation time. Heat extraction declines with time. For instance, after 5 years of operation, simulated values of the SD scenarios are 92 W/m (base case 3) to 113 W/m

(base case 4), and 73 W/m (base case 1) to 97 W/m (base case 2) of the NS scenarios, respectively. The heat extraction rates from the base cases are listed in Table 5.
Total thermal power of the DBHE is highest for base case 1 and 2. One reason is that the maximal re-completion depth of the well with a 7" casing is 4.3 km for base cases 1 and 2 and only 2.8 km for the wells through the salt diapir (base cases 3 and 4). Another reason is the higher intersection length with the highly conductive Zechstein salt in base cases 3 and 4 compared to base cases 1 and 2. The third reason is the higher geothermal gradient in the region of the SD well. If we compare the two re-completion schemes, it is clear that the base cases 2 and 4 with operation parameters and composite tubing of Arnsberg yield higher predicted thermal output than base cases 1 and 3. One reason for this is the flow rate, which is higher in the Arnsberg setting. The sensitivities of each parameter are described more thoroughly in section 3.1.1.
Comparing the simulation results of this study to the values given by the Bundesverband Geothermie, it should be possible to extract even more thermal power. To test this, we used the well through a normal stratigraphic setting and re-completed it with the parameters listed as "high case" (Table 5) scenario with a vacuum insulated tubing comparable to the one installed in the Eden geothermal project (Cornwall, UK), we reduced the injection temperature to 15 °C (as for the DBHE in Prenzlau, and to inhibit cooling of the injected water in the uppermost kilometer) and increased the flow rate to 5 l/s according to our simulation results of this study. With this set of parameters, the model predicts a total thermal output of 600 kW and a thermal output per unit length of 139.7 W/m. With this result, the values given by the Bundesverband Geothermie are almost reached and are in the same order of magnitude between 100 and 600 KW as described in Wight und Bennett 2015).

*Table 5: Summary of the results of four base cases and real cases Prenzlau, Weggis and Arnsberg. For comparison one "high case" with the re-completion scheme with a vacuum insulated tubing. * values according to the "natural circulation", without a heat pump.*

Parameter [Unit]	Prenz lau	Wegg is	Arns-berg	1	2	3	4	NS VIT
	Real cases			Base cases				High Case
Total depth [m]	2.8	2.3	2.8	4.3	4.3	2.8	2.8	4.3
Temperature at total depth [°C]	108	78	90	139	139	114	114	139
T_i [°C]	15	35	40	35	40	35	40	15
Flow rate [l/s]	3.3	1.7	3.1	1.7	3.1	1.7	3.1	5
T_o [°C]	50	41	48					

T_o after 5 years of operation time[°C]				78	72.2	69.2	64	
T_o after 30 years of operation time[°C]				74	68.7	66.6	61.7	
P [kW]	120 *	42	102					
P after 5 years of operation time [kW]				313	417	258	317	
P after 30 years of operation time [kW]				294	376	241	287	600.5
Heat extraction rates per meter-age after 5 years [W/m]				73	97	92	113	
Heat extraction rates per meter-age after 30 years [W/m]	42.9	18.3	36.4	68	87.4	86	102.5	139.7

To understand the processes and estimate the quality of the heat source of recompleted idle wells in the NGB, we compare the results and parameters with three known real cases: Prenzlau, Arnsberg, and Weggis (Table 5). To compare only cases without heat pump, we decided to use the "natural circulation" scenario for Prenzlau. However, the real thermal output is nearly four times higher because of the involved heat pump.

We calculated the thermal power for the real cases with Equation 3. The thermal power of Prenzlau with 120 kW, Weggis with 42 kW and Arnsberg with 102 kW are less than half of the predicted heat extraction rates for the base cases in this study. One reason is that the temperature at total depth of 114 °C (base case 3 and 4) and 139 °C (base case 1 and 2) are higher than in Prenzlau (108 °C), Weggis (78 °C) and Arnsberg (90 °C). The total depth of the wells in base cases 3 and 4 is comparable with the total depth in Prenzlau and Arnsberg. Comparing the heat extraction rate per unit length of the Arnsberg DBHE (36.4 W/m) with the re-completion scheme of Arnsberg in base cases 2 (87.4 W/m) and 4 (102.5 W/m) of this study yields huge differences by a factor of two for base case 2 and a factor of three for base case 4. one reason for higher values in base case 2 of the NS well location is that the calculated values of the re-completion depth is to 4.3 km with the re-completion scheme of the Arnsberg BHE. The operation data of relatively high reinjection temperature and high flow rates are optimized for the setting of base case 2 with a longer well. Additional parameters could influence the heat extraction rate, but are not further investigated in this study.The increased geothermal gradient at the well location of the salt diapir is one parameter leading to higher extraction rates in base case 4.

The presented DBHE models have some limitations leading to uncertainties in the predicted thermal power of the re-completed idle wells.

Two parts need to be discussed separately. On the one hand, the upper part of the DBHE needs to be well isolated if the reinjection temperature is above the groundwater temperature. With the simulation software FEFLOW, this is impossible to implement, and as this study is focusing on very deep wells, this effect is also minor. However, it reduces the predicted thermal output of the cases if the injection temperatures is above 15 °C. On the other hand, the idle wells are well isolated in the upper hundreds and sometimes even thousands of meters because several casings filled with fluids or cement already exist. The effect is underestimated in the numerical simulations, meaning that thermal power in reality should be even higher. In the base cases, the reduction is visible because injection temperatures are higher than groundwater temperatures, but for scenarios with 5 and 10 °C, the predicted thermal output is not reduced.

For this feasibility study all parameters were held constant and only one parameter was adjusted in the given parameter ranges. The correlations between the different parameters cannot be discussed with this workflow. For such an estimate of correlations, a global sensitivity study would be needed (e.g. Saltelli 2004. However, meaningful global sensitivity studies with the number of parameters considered here would require thousands of forward simulations – and, therefore, be infeasible with the current implementation. Such an approach would be possible with suitable surrogate models (e.g. Degen et al. 2019; Degen et al. 2021) and this is an interesting path for future research.

With this study we could show that the re-completion depth has the highest impact on the thermal output of the DBHE. This is also valid for the total thermal output and the output per unit length. This finding is in agreement with the study of Holmberg et al. (2016), who state that the thermal performance of coaxial BHE is significantly increased with depths. Also in Gascuel et al. (2022), the performance of DBHE and energy extraction per meterage was shown to increase with the BHE depth.

In Nian et al. (2019) the depths of the well is only the second most important sensitive parameter influencing the performance of the system. There the most important factor is the flow rate, while it is important to mention, that they assessed the sensitivity of the COP not the thermal output without heat pump. The exact opposite is postulated in Pan et al. (2019) where the mass flow has a low sensitivity on the production temperature. But it is important to mention, that only flow rates above 8 kg/s are simulated in Pan et al. (2019). And as we could present in this study, the flow rate has its highest sensitivity between 1.5 l/s and 5 l/s, higher values of flow rate have low influence on the predicted thermal output, as well as production temperature.

Important is, that the maximal re-completion depth is a given constant for each location, which is only possible to optimize in the project phase of selecting individual idle wells to be re-completed. This is different from the injection temperature, which is the second most important parameter to increase or to reduce the thermal output. As this is an operation parameter, it can be optimized for the needed temperature level of the heat grid.

The amount of heat that can be extracted also depends on the consumer's demand. If more heat is consumed, the heat generation costs decrease while the operating hours increase. Therefore, it would be beneficial to integrate these DBHE for one consumer

meeting high operating hours or into a 4th or 5th generation heat grid that operates on temperatures around 60 °C. The DBHE would then operate as a base load, providing energy for the entire year. If the DBHE only supplies a small number of buildings, the operating hours will decline in the summer due to the low heat demand. These low operating hours would supply the analyzed consumers from Section 3.2.1, leading to a less economical solution. If the complete area of the SD well location (~ 176 GWh/a) is supplied by the well (~ 2.4 GWh/a) in a combined district heating system, high operating hours will be possible, leading to a more economical solution. Supplying only one consumer with high operating hours will always be the most economical system due to lower equipment costs for distributing the heat between different buildings. However, this is not a feasible solution for a roll-out of many idle wells and will remain a rare possibility.

If high operating hours are ensured, the DBHE heat generation costs at the wellhead are competitive against other renewable technologies, e.g. solar-thermal energy (Maaß und Sandrock 2016). Due to rising gas prices, they are also competing against gas boilers for higher distances, as shown in the first and second base cases.

The quality of the heat source of a DBHE is summarized and visualized in Figure 20. The findings of this study quantified the influence of the distance between the repurposed idle well (as heat source) and the consumer, and within the heat demand mapping of the two individual locations of the wellbores, it was shown that the distance is high. Moreover, it was shown that the heat source is the most valid and has the lowest heat generating costs, when the availability is highest. The DBHE should be operated for the entire year with 8000 h (Figure 16, Figure 17, Figure 18 and Figure 19).

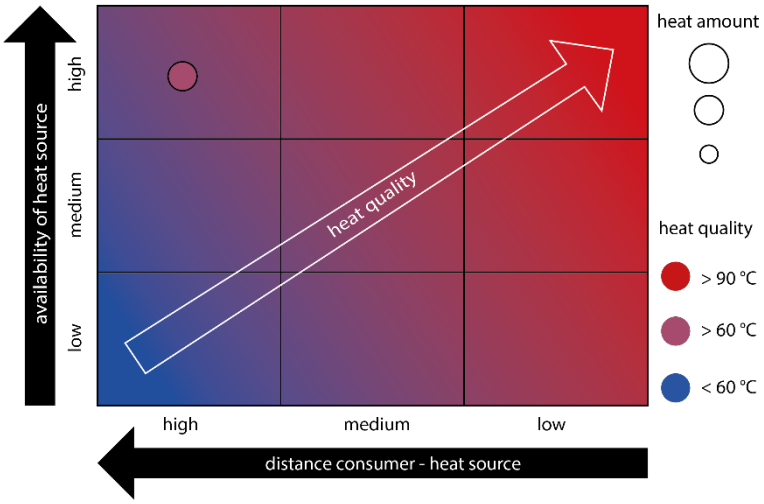

Figure 20 The quality of the DBHE as heat source can be assessed on ranking it depending on the availability, and the distance between the consumer and the heat source.

In general, it is possible to calculate heat generation costs, and thereby the economic value of the re-completed heat source is possible in two different ways of implementation of the well as heat source in a heat grid (Figure 21).

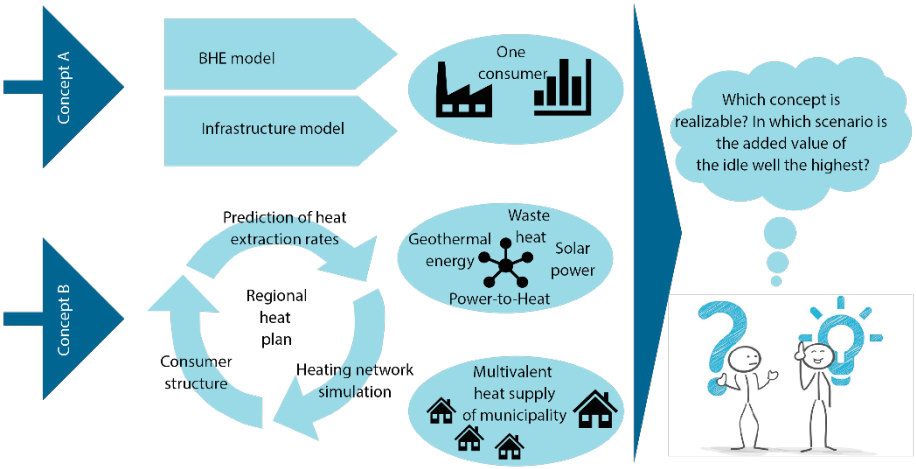

Figure 21: Two different conceptualized workflows to use the heat from re-completed idle wells as deep borehole heat exchangers (deep BHE).

This feasibility study follows concept A in Figure 21, which is straight forward and beneficial if the existing infrastructure can be used and the heat source is the only source for the consumers. Within concept A, heat is directly transported via the heat grid to the consumer. In this concept, heat production costs are minimized if the consumer uses the heat source during the entire year (for example, for indoor swimming pools), and the heat demand of the consumer has a minimal difference between base load and peak load. An alternative scheme for efficiently using DBHE from repurposed idle wells is integrating one heat source (besides others like solar power or waste heat) in a regional heat plan for an entire municipality. As part of a fourth generation district heating (4GDH) system (Formhals et al. 2021) or even an Ultra-Low Temperature District Heating and Cooling (ULTDHC) (Quirosa et al. 2023; Buffa et al. 2019) multivalent heating grid. This heat source (the operation parameter of the BHE) could be optimized for rather low production temperatures, resulting in very high thermal power. This concept (Concept B in Figure 21) is a multivalent heat supply approach, combining heat sources and sinks in an intelligent heating and cooling network. The best choice depends on the location and availability of heat supply and demand at the location of the repurposed well.

5 Conclusion

Our study confirms that repurposing of idle wells as deep borehole heat exchangers can be economic. The initial production costs for heat calculated in this study are comparable to other renewable energy resources like biomass and - depending on distance between source and user – also competitive with current natural gas prices. The distance between the well and consumer should not be greater than 3 km to 5 km to minimize the costs for pipelines, which are factored into the simulation of heat production costs and moreover, to avoid cooling of the working fluid. Additionally, it is essential to

produce heat at a temperature of more than 60 °C to ensure that no heat pumps are required for the end user. To use the DBHE most efficiently, it is important to operate the heat source for 8000 hours per year (i.e., not only during winter).

It can be concluded that repurposing deep idle wells as DBHE would be a valuable heat source for district heating networks. The comprehensive workflow of this study makes it possible to state general arguments and suggestions how to proceed with the recompletion and value-added strategy for idle wells of the oil and gas industry.

1. Overall, the heat extraction rate and the production temperature are increasing linearly with re-completing depth. Therefore, preferably idle wells where the 7" surface casing is deepest should be the main target to repurpose as DBHE.
2. High geothermal gradients and surrounding rocks with high thermal conductivity like in the Zechstein salt are beneficial for high heat extraction rates of the DBHE over the lifetime of 30 years.
3. To guarantee the best economic performance, the heat source should be operated constantly over the entire year with 8000 operating hours. This minimizes heat generation costs and makes it comparable to other heat sources. Operation of the DBHE through the entire year is only possible with direct consumers of very uniform heat demand or by integrating this heat source in a 4^{th} or 5^{th} generation heat grids as a base load contribution.
4. The extraction rate at the well head has to be designed within an extensive district heating system, including other energy converters and storage units, and with regard to the demand structure to ensure sufficient temperatures at the household stations. The temperature at the consumer should not be lower than 60 °C. The optimization of the DBHE is not only possible by increasing the heat extraction rate. Because, reducing the inflow temperature and increasing the flow rate, the heat extraction rate is increased but consequently the production temperature is reduced and the quality of the heat source is reduced (Figure 20). Therefore, the optimization of the DBHE should be done in parallel to the heating network where the heating demand should be directly included.
5. The distance from the DBHE to the consumer should not be higher than 3 km. The main reason to prefer small distances are the high costs of the heating networks. With higher distances the heat costs for the consumer are rapidly increasing and the system will become ineconomic.

6 List of abbreviations

ULTDHC	Ultra-Low Temperature District Heating and Cooling
4GDH	Fourth generation district heating system
BHE	Borehole heat exchanger
DBHE	Deep borehole heat exchanger

SD	Salt diapir setting
NS	Normal stratigraphic setting
VIT	Vacuum insulated tubing
GFK	Glass-fiber reinforced plastic material
AGEB	AG Energiebilanzen e.V.
TRY	Test Reference Year

7 Declarations

7.1 Data availability

The datasets generated and analyzed during the current study are not publicly available but are available from the corresponding author on reasonable request.

7.2 Competing interests

The authors declare that they have no competing interests

7.3 Funding

This study was funded by the company ExxonMobil Production Deutschland GmbH. The results of this study are published with financial addition of the Fraunhofer IEG.

7.4 ”Authors’ contributions

NK wrote the manuscript with the input from all coauthors. NK simulated the heat exchanger. NK and JS conceptualized the study. JS prepared the geological data base and selected the well locations. MS did the heating grid simulation and calculated the heat generating costs. JN revised the manuscript. FW revised manuscript and results of simulations and sensitivity analyses.

7.5 Acknowledgements

We are thankful for the input and heat demand mapping of the competence center *Integrated District Planning* of Fraunhofer IEG, especially Sebastian Steininger and Kai George.

Deepest gratitude goes to the competence center *deep drilling technologies and completion* of Fraunhofer IEG, Dimitra Teza and Dirk Boernecke brought all the drilling engineering know-how which is important for the realistic parametrization of the BHE re-completion. We thank Marcel Halm from Fraunhofer IEG *Near-Surface Geothermal Energy* for assisting in the simulation work with FEFLOW.

We are thankful for the substantive exchange with the Eden Geothermal Project to learn how the deep BHE was re-completed in Cornwall, UK.

Literaturverzeichnis

Agemar, Thorsten; Schellschmidt, Rüdiger; Schulz, Rüdiger (2012): Subsurface temperature distribution in Germany. In: *Geothermics* 44, S. 65–77.

Alimonti, Claudio; Soldo, Elena; Bocchetti, D.; Berardi, Danielle M. (2018): The wellbore heat exchangers: A technical review. In: *Renewable Energy*.

Bayer, U.; Scheck, M.; Koehler, M. (1997): Modeling of the 3D thermal field in the northeast German basin. In: *Geologische Rundschau* (86), S. 241–251.

Brown, Christopher S.; Cassidy, Nigel J.; Egan, Stuart S.; Griffiths, Dan (2021): Numerical modelling of deep coaxial borehole heat exchangers in the Cheshire Basin, UK. In: *Computers & Geosciences* 152, S. 104752. DOI: 10.1016/j.cageo.2021.104752.

Buffa, Simone; Cozzini, Marco; D'Antoni, Matteo; Baratieri, Marco; Fedrizzi, Roberto (2019): 5th generation district heating and cooling systems: A review of existing cases in Europe. In: *Renewable and Sustainable Energy Reviews* 104, S. 504–522. DOI: 10.1016/j.rser.2018.12.059.

Bundesverband Geothermie: Tiefe Geothermie. Online verfügbar unter https://www.geothermie.de/geothermie/geothermische-technologien/tiefe-geothermie.html, zuletzt geprüft am 22.02.2023.

Bundesverband Geothermie (2023): AACHEN SUPER C. Lexikon der Geothermie. Online verfügbar unter https://www.geothermie.de/bibliothek/lexikon-der-geothermie/a/aachen.html, zuletzt aktualisiert am April 2023, zuletzt geprüft am 15.09.2023.

Degen, Denise; Veroy, Karen; Freymark, Jessica; Scheck-Wenderoth, Magdalena; Poulet, Thomas; Wellmann, Florian (2021): Global sensitivity analysis to optimize basin-scale conductive model calibration – A case study from the Upper Rhine Graben. In: *Geothermics* 95, S. 102143. DOI: 10.1016/j.geothermics.2021.102143.

Degen, Denise; Veroy, Karen; Wellmann, Florian (2019): Certified Reduced Basis Method in Geosciences Addressing the challenge of high dimensional problems.

Deutscher Wetterdienst (DWD), Bundesamt für Bauwesen und Raumordnung (BBR) (2017): Ortsgenaue Testreferenzjahre von Deutschland für mittlere, extreme und zukünftige Witterungsverhältbisse. Handbuch.

DHI Wasy: Feflow 7.2 Documentation - Rate-Budget Panel. Online verfügbar unter http://www.feflow.info/html/help72/feflow/14_References/GUI/Panels/panel_rate_budget.html, zuletzt geprüft am 22.02.2023.

DHI Wasy: Feflow 7.3 Documentation. BHE Dataset Editor. Online verfügbar unter http://www.feflow.info/html/help73/feflow/14_References/GUI/Dialogs/bhe_dataset_editor.html, zuletzt geprüft am 22.02.2023.

Diersch, H.J.G. (2013): FEFLOW: Finite Element Modeling of Flow, Mass and Heat Transport in Porous and Fractured Media: Springer Berlin Heidelberg. Online verfügbar unter https://books.google.de/books?id=ZXXABAAAQBAJ.

Diersch, H.J.G.; Bauer, D.; Heidemann, W.; Rühaak, Wolfram; Schätzl, Peter (2010): Finite element formulation for borehole heat exchangers in modeling geothermal heating systems by FEFLOW. In: *WASY Software FEFLOW White Paper* 5, S. 5–96.

Diersch, H.-J.G.; Bauer, D.; Heidemann, W.; Rühaak, W.; Schätzl, P. (2011): Finite element modeling of borehole heat exchanger systems. In: *Computers & Geosciences* 37 (8), S. 1136–1147. DOI: 10.1016/j.cageo.2010.08.002.

Eskilson, Per; Claesson, Johan (1988): SIMULATION MODEL FOR THERMALLY INTERACTING HEAT EXTRACTION BOREHOLES. In: *Numerical Heat Transfer* 13 (2), S. 149–165. DOI: 10.1080/10407788808913609.

Eugster, Walter; Füglister, Hans (2001): Tiefe Erdwärmesonde Weggis. Messkampagne zur Dokumentierung der neuen Einflüsse beim Ausbau der Ab-nehmerleistung. Zürich. Online verfügbar unter https://www.aramis.admin.ch/Default?DocumentID=64252&Load=true, zuletzt geprüft am 22.02.2023.

FEFLOW. Finite Element Modeling of Flow, Mass and Heat Transport in Porous and Fractured Media (2014). Aufl. 2014. Berlin, Heidelberg: Springer Berlin Heidelberg.

Formhals, Julian; Feike, Frederik; Hemmatabady, Hoofar; Welsch, Bastian; Sass, Ingo (2021): Strategies for a transition towards a solar district heating grid with integrated seasonal geothermal energy storage. In: *Energy* 228, S. 120662. DOI: 10.1016/j.energy.2021.120662.

Frick, Maximilian (2019): Towards a more sustainable utilization of the urban geological subsurface: Insights from 3D thermohydraulic models. Freie Universität Berlin.

Frick, Maximilian; Scheck-Wenderoth, Magdalena; Schneider, Michael; Cacace, Mauro (2019): Surface to Groundwater Interactions beneath the City of Berlin: Results from 3D Models. In: *Geofluids* 2019, S. 1–22. DOI: 10.1155/2019/4129016.

Fromme, Kirsten; Michalzik, Dieter; Wirth, Wolfgang (2010): Das geothermische Potenzial von Salzstrukturen in Norddeutschland. In: *ZDGG* 161 (3), S. 323–333. Online verfügbar unter file:///C:/Users/nor82818/Downloads/zdgg_Band_161_Heft_3_p323-333_The_geothermal_potential_of_salt_structures_in_Northern_Germany_75317.pdf.

Garcin, Jean (2016): Dynamische Simulation von Optimierungsstrategien zur Tiefen Erdwärmesonde Arnsberg-Erlenbach 2. Masterarbeit. Technische Universität München. München.

Gascuel, Violaine; Raymond, Jasmin; Rivard, Christine; Marcil, Jean-Sébastien; Comeau, Félix-Antoine (2022): Design and optimization of deep coaxial borehole heat exchangers for cold sedimentary basins. In: *Geothermics* 105, S. 102504. DOI: 10.1016/j.geothermics.2022.102504.

Geiger, B.; Kleeberger, Heinrich; Hardi, Lukas (2019): Erstellen der Anwendungsbilanzen 2013 bis 2017 für den Sektor Gewerbe, Handel, Dienstleistungen (GHD). Hg. v. Arbeitsgemeinschaft Energiebilanzen e.V. Lehrstuhl für Energiewirtschaft und Anwendungstechnik Technische Universität München. Berlin.

Glück, Bernd (1985): Heizwassernetze für Wohn- und Industriegebiete. Frankfurt (Main): Verl.- u. Wirtschaftsges. der Elektrizitätswerke mbH.

Holmberg, Henrik; Acuña, José; Næss, Erling; Sønju, Otto K. (2016): Thermal evaluation of coaxial deep borehole heat exchangers. In: *Renewable Energy* 97, S. 65–76. DOI: 10.1016/j.renene.2016.05.048.

Houska, Treva (2012): EarthExplorer. Unter Mitarbeit von U.S. Geological Survey. Reston, VA (General Information Product, 136). Online verfügbar unter http://pubs.er.usgs.gov/publication/gip136.

Kohl, Thomas; Brenni, Renzo; Eugster, Walter (2002): System performance of a deep borehole heat exchanger. In: *Geothermics* 31 (6), S. 687–708. DOI: 10.1016/S0375-6505(02)00031-7.

Le Lous, Morgan; Larroque, François; Dupuy, Alain; Moignard, Adeline (2015): Thermal performance of a deep borehole heat exchanger: Insights from a synthetic coupled heat and flow model. In: *Geothermics* 57, S. 157–172. DOI: 10.1016/j.geothermics.2015.06.014.

Linda Lilburne; Stefano Tarantola (2009): Sensitivity analysis of spatial models. In: *Int. J. Geogr. Inf. Sci.* 23 (2), S. 151–168. DOI: 10.1080/13658810802094995.

Liu, Jun; Wang, Fenghao; Cai, Wanlong; Wang, Zhihua; Wei, Qingpeng; Deng, Jiewen (2019): Numerical study on the effects of design parameters on the heat transfer performance of coaxial deep borehole heat exchanger. In: *Int J Energy Res* 43 (12), S. 6337–6352. DOI: 10.1002/er.4357.

Maaß, Christian; Sandrock, Matthias (2016): Förder- und Finanzierungsleitfaden für Freiflächen- Solarthermie-Anlagen mit Wärmespeicher und Anbindung an Wärmenetze. Hamburg Institut. Online verfügbar unter https://www.hamburg-institut.com/wp-content/uploads/2021/07/Foerderleitfaden_Freiflaechen-Solarthermie.pdf, zuletzt geprüft am 13.02.2023.

Magri, Fabien; Bayer, Ulf; Tesmer, Maja; Möller, Peter; Pekdeger, Asaf (2008): Salinization problems in the NEGB: results from thermohaline simulations. In: *Int J Earth Sci (Geol Rundsch)* 97 (5), S. 1075–1085. DOI: 10.1007/s00531-007-0209-8.

Michalzik, D.; Fromme, K.; Nowag, S. (2010): Machbarkeitsstudie: Tiefe Erdwärmesonde Bad Laer: Abschlussbericht ; [Projektbeginn: 28.04.2009; Projektende: 28.12.2009]: Gesundheitszentrum Bad Laer GmbH. Online verfügbar unter https://books.google.de/books?id=rwt7mwEACAAJ.

Nian, Yong-Le; Cheng, Wen-Long; Yang, Xing-Yu; Xie, Kun (2019): Simulation of a novel deep ground source heat pump system using abandoned oil wells with coaxial

BHE. In: *International Journal of Heat and Mass Transfer* 137, S. 400–412. DOI: 10.1016/j.ijheatmasstransfer.2019.03.136.

Noack, Vera; Scheck-Wenderoth, Magdalena; Cacace, Mauro; Schneider, Michael (2013): Influence of fluid flow on the regional thermal field: results from 3D numerical modelling for the area of Brandenburg (North German Basin). In: *Environ Earth Sci* 70 (8), S. 3523–3544. DOI: 10.1007/s12665-013-2438-4.

Pan, Aiqiang; Lu, Lin; Cui, Ping; Jia, Linrui (2019): A new analytical heat transfer model for deep borehole heat exchangers with coaxial tubes. In: *International Journal of Heat and Mass Transfer* 141, S. 1056–1065. DOI: 10.1016/j.ijheatmasstransfer.2019.07.041.

Quirosa, Gonzalo; Torres, Miguel; Becerra, José A.; Jiménez-Espadafor, Francisco J.; Chacartegui, Ricardo (2023): Energy analysis of an ultra-low temperature district heating and cooling system with coaxial borehole heat exchangers. In: *Energy* 278, S. 127885. DOI: 10.1016/j.energy.2023.127885.

Rashid, Farhan Lafta; Dhaidan, Nabeel S.; Hussein, Ahmed Kadhim; Al-Mousawi, Fadhel Noraldeen; Younis, Obai (2023): Ground heat exchanger in different configuration: Review of recent advances and development. In: *Geoenergy Science and Engineering* 227, S. 211872. DOI: 10.1016/j.geoen.2023.211872.

Rheinisch-Westfälische Technische Hochschule Aachen (2011): Erste Ergebnisse zur Betriebsintegration der Erdwärmesonde am SuperC in Aachen. Hg. v. Energieexperten.org. Online verfügbar unter https://www.energie-experten.org/news/erste-ergebnisse-zur-betriebsintegration-der-erdwaermesonde-am-superc-in-aachen, zuletzt aktualisiert am 26.07.2011, zuletzt geprüft am 15.09.2023.

Saltelli, Andrea (2004): Global sensitivity analysis: An introduction. In: *Proceedings of the 4th international conference on sensitivity analysis of model output (SAMO 2004)*.

Santos, L.; Dahi Taleghani, A.; Elsworth, D. (2022): Repurposing abandoned wells for geothermal energy: Current status and future prospects. In: *Renewable Energy* 194, S. 1288–1302. DOI: 10.1016/j.renene.2022.05.138.

Sharmin, Tasnuva; Khan, Nazia Rodoshi; Akram, Md Saleh; Ehsan, M. Monjurul (2023): A State-of-the-Art Review on Geothermal Energy Extraction, Utilization, and Improvement Strategies: Conventional, Hybridized, and Enhanced Geothermal Systems. In: *International Journal of Thermofluids* 18, S. 100323. DOI: 10.1016/j.ijft.2023.100323.

Sobol′, I.M (2001): Global sensitivity indices for nonlinear mathematical models and their Monte Carlo estimates. In: *Mathematics and Computers in Simulation* 55 (1), S. 271–280. DOI: 10.1016/S0378-4754(00)00270-6.

Sporleder, Maximilian; Rath, Michael; Ragwitz, Mario (2022): Design optimization of district heating systems: A review. In: *Front. Energy Res.* 10, Artikel 971912. DOI: 10.3389/fenrg.2022.971912.

Steinbach, Jan; Popovski, Eftim; Henrich, Jasmin; Christ, Catrice; Ortner, Sara; Pehnt, Martin et al. (2020): Umfassende Bewertung des Potenzials für eine effiziente Wärme- und Kältenutzung für Deutschland. Online verfügbar unter https://i-rees.de/wp-content/uploads/2021/03/Comprehensive-Assessment-Heating-and-Cooling_Germany_2020.pdf, zuletzt geprüft am 12.01.2022.

Stober, Ingrid; Bucher, Kurt (2020): Geothermie. Berlin, Heidelberg: Springer Berlin Heidelberg.

Verenum (2017): Planungshandbuch Fernwärme. Version 1.1 vom 21. September 2017. Ittigen, Bern: EnergieSchweiz Bundesamt für Energie.

Wainwright, Haruko M.; Finsterle, Stefan; Jung, Yoojin; Zhou, Quanlin; Birkholzer, Jens T. (2014): Making sense of global sensitivity analyses. In: *Computers & Geosciences* 65, S. 84–94. DOI: 10.1016/j.cageo.2013.06.006.

Wenderoth, F.; Fritzer, T.; Gropius, M.; Huber, B.; Schubert, A. (2005): Numerische 3D-modellierung eines geohydrothermalen dublettenbetriebs im malmkarst. In: *Geothermische Energie* 48 (2005), S. 16–21.

Wight, N. M.; Bennett, N. S. (2015): Geothermal energy from abandoned oil and gas wells using water in combination with a closed wellbore. In: *Applied Thermal Engineering* 89, S. 908–915. DOI: 10.1016/j.applthermaleng.2015.06.030.

8 Supplementary Material S1: Rock Poroperties

Table 6: Depth of main stratigraphic units from the bore logs are used as subhorizontal layers for the numerical models. NS = Normal stratigraphic setting model, SD = Salt diapir model. With the physical rock properties: n = porosity, λ= thermal conductivity of the solid, c= volumetric heat capacity, H_s = Radiogenic heat production. Property values after the following references: 1) Noack et al. (2013), 2) Bär (2012), 3) Magri et al. (2008), 4) Bayer et al. (1997), 5) Frick (2019) and 6) Frick et al. (2019)

	NS well						SD well					
Name	Top [m]	Base [m]	n [-]	λ [W/m/K]	c [MJ/m^3/K]	H_s [µW/m^3]	Top [m]	Base [m]	n [-]	λ [W/m/K]	c [MJ/m^3/K]	H_s [µW/m^3]
Quaternary	25.52	-52.48	0.26 [3]	1.5 [3]	3.1 [3]	0.7 [1]	71.8	-63	0.26 [3]	1.5 [3]	3.1 [3]	0.7 [1]
Tertiary	-52.48	-889.48	0.23 [1]	1.5 [4]	2.4 [3]	0.3 [1]	-63	-380	0.23 [1]	1.5 [4]	2.4 [3]	0.3 [1]
Cretaceous	-889.48	-2432.48	0.1 [3]	2 [4]	1.95 [3]	0.85 [1]	-380	-587	0.1 [3]	2 [4]	1.95 [3]	0.85 [1]
Keuper	-2432.48	-2861.48	0.06 [3]	2.3 [4]	2.32 [5]	1.4 [4]	-587	-680	0.06 [3]	2.3 [4]	2.32 [5]	1.4 [4]
Muschelkalk	-2861.48	-3168.48	0.1 [5]	1.9 [4]	2.25 [5]	0.3 [4]	-680	-909	0.1 [5]	1.9 [4]	2.25 [5]	0.3 [4]
Upper Buntsandstein	-3168.48	-3446.48	0.0250 [6]	3 [6]	2.19 [6]	1.8 [5]	-	-	-	-	-	-
Middle and lower Buntsandstein	-3446.48	-3959.48	0.092 [6]	1.92 [6]	2.39 [6]	1.8 [5]	-	-	-	-	-	-
Buntsandstein	-	-	-	-	-	-	-909	-982	0.04 [3]	2 [4]	2.4 [3]	1.8 [5]
Zechstein salt	-	-	0.005 [5]	4.5 [5]	1.94 [5]	0.09 [4]	-982	-1002	0.005 [5]	4.5 [5]	1.94 [5]	0.09 [4]

Buntsandstein	-		-	-	-	1.8 [5]	-1002	-1752	0.04 [3]	2 [4]	2.4 [3]	1.8 [5]
Zechstein salt	-3959.48	-4329.78	0.005 [5]	4.5 [5]	1.94 [5]	0.09 [4]	-1752	-2913.9	0.005 [5]	4.5 [5]	1.94 [5]	0.09 [4]
Zechstein salt	-4329.78	-4551.28	0.005 [5]	4.5 [5]	1.94 [5]	0.09 [4]	-2913.9	-4433	0.005 [5]	4.5 [5]	1.94 [5]	0.09 [4]
Rotliegend	-4551.28	-5304.98	0.09 [2]	2.25 [4]	2 [2]	1 [4]	-4433	-4663	0.09 [2]	2.25 [4]	2 [2]	1 [4]
Model base		-5500						-5000				

9 Supplementary Material S2: Equations to solve coaxial BHE in FEFLOW

The geometry type for the BHE in our simulations is set to a coaxial probe with an annular inlet and its material-specific heat-transfer coefficients are calculated from its different components, namely the declared thermal conductivity and geometry of the tubing (denoted as t), the casing (denoted as c) and the grout zone (denoted as g) (DHI Wasy).

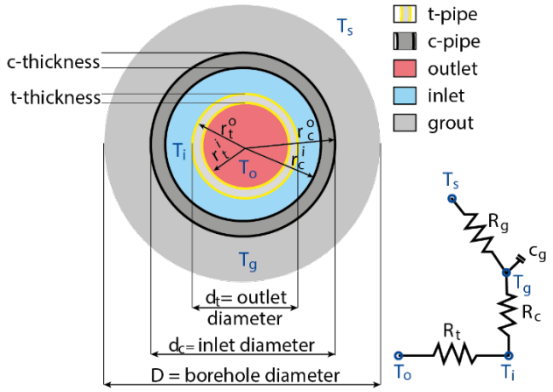

Figure 22: Thermal resistance (R) couples the different components of temperature levels (T) in the pipes (subscripts c = casing; t = tubing), grout (subscript g) and soil (subscript s). Adopted from (Diersch et al. 2011)

As computational approach we use the provided quasi-stationary method (Eskilson und Claesson 1988), which is a simplified analytical method assuming a local thermal equilibrium between the elements of the BHE. This method is well fitted for long term analyses with few changes in inflow temperatures of the BHE and is reasonably accurate in comparison to the numerical approach while also providing a low computational cost. Since in the analytical BHE method the inherent transfer conditions are dependent on the soil temperatures, an iterative procedure is required (DHI Wasy).

The equations to solve the coaxial BHE in FEFLOW is implemented after (Diersch et al. 2011) with the heat source /sink (H) of the three components form the outlet, the inlet and the grout zone:

Equation 7

$$\frac{\partial}{\partial_t}(\rho^r c^r T_o) + \nabla \cdot (\rho^r c^r \boldsymbol{u} T_o) - \nabla \cdot (\Lambda^r \cdot \nabla T_o) = H_o$$

With:

Equation 8

$$q_{nTo} = -\Phi_t(T_i - T_o)$$

Equation 9

$$\frac{\partial}{\partial_t}(\rho^r c^r T_i) + \nabla \cdot (\rho^r c^r \boldsymbol{u} T_i) - \nabla \cdot (\Lambda^r \cdot \nabla T_i) = H_i$$

With:

Equation 10

$$q_{nTi} = -\Phi_c(T_g - T_i) - \Phi_t(T_o - T_i)$$

Equation 11

$$\frac{\partial}{\partial_t}(n_g \rho^g c^g T_g) - \nabla \cdot (n_g \lambda^g \nabla T_g) = H_g$$

With:

Equation 12

$$q_{nTg} = -\Phi_g(T_S - T_g) - \Phi_c(T_i - T_g)$$

where the superscript r is the refrigerant, **u** the velocity vector of the circulating refrigerant, Φ denotes the heat transfer coefficient. The subscript t corresponds to the tubing and c corresponds to the casing. The subscript g corresponds to the grout while subscripts i means inlet and o means outlet pipe (see also Figure 22).

The thermal resistance R (in Figure 22) is a measure of the ability of an installation to resist heat transfer via its surface. In a coaxial BHE the thermal resistance is comprised of the resistance due to the advective flow of the refrigerant in the pipes, due to the pipe wall material and grout transition and due to grout-soil exchange. It is determined from the geometry and material of the three different component zones (Diersch et al. 2011).

The heat transfer coefficients Φ are related to thermal resistance relationships R to express the effective coefficient for each the specific exchange surface S after (Diersch et al. 2011) as follows:

Equation 13

$$\Phi_t = \frac{1}{R_t} \cdot \frac{1}{S_t}$$

Equation 14

$$\Phi_c = \frac{1}{R_c} \cdot \frac{1}{S_c}$$

Equation 15

$$\Phi_g = \frac{1}{R_g} \cdot \frac{1}{S_g}$$

The surfaces are calculated for the coaxial BHE as:

Equation 16

$$S_t = r_t^i 2\pi$$

Equation 17

$$S_c = r_c^i 2\pi$$

Equation 18

$$S_g = D\pi$$